A STUDY OF FRACTURE CONDUCTIVITY IN CARBONATE ROCK CREATED BY ACID AND PROPPANT

A Thesis

by

ALEXANDER FOJTASEK

Submitted to the Graduate and Professional School of
Texas A&M University
in partial fulfillment of the requirements for the degree of

MASTER OF SCIENCE

Chair of Committee,	A. Daniel Hill
Committee Members,	Ding Zhu
	Arthur Donovan
Head of Department,	Jeff Spath

May 2022

Major Subject: Petroleum Engineering

ABSTRACT

Today the majority of onshore United States oil production comes from unconventional reservoirs that have very low permeability and porosity, such as the Austin Chalk formation, and require stimulation methods to produce economically. A very common method is hydraulic fracturing, which can be split up into proppant supported fractures and acid etched fractures. The cost of hydraulic fracturing depends on the type of fluid used as well the type of proppant. The proppant holds the created fracture network open after pumping has ceased and the closure stress of the reservoir is applied to the fracture network, allowing reservoir fluid to flow to the wellbore. Acid etched fractures apply the same principles as proppant supported fractures except that acid etched fractures rely on high points left after acid has dissolved the fracture surface to hold the fracture open.

A 40/70 mesh sand provided by SM Energy was tested for this study. Acid fracture conductivity created using 15% hydrochloric acid was also tested and compared with the propped fracture conductivity. Samples were tested that were acid fractured with 15% hydrochloric acid at 10-minute and 20-minute residence times and then propped with proppant using a concentration of 0.2 lb_m/ft^2.

The ability of fluid to flow through the fracture network to the wellbore is called fracture conductivity and it can be used to describe how successful a hydraulic fracture treatment has been or predicted to be if modeled. Dimensionless fracture conductivity is the ratio of the fracture's ability to transport fluid through the fracture over the

reservoir's ability to transport fluid to the fracture. It is used to evaluate and optimize hydraulic fracture design. American Petroleum Institute Recommended Practice 61 procedures guided the conductivity testing of all the samples. This is the recommended practice for evaluating short term conductivity of propped and acid etched samples and has been put in place by the American Petroleum Institute. Proppant is the solid used in hydraulic fracturing that props the fracture open after pumping of the hydraulic fluid has stopped and the reservoir closure stress is applied to the fracture. The same concepts apply to acid etched surfaces where incongruent high points and dissolved faces hold the fracture open.

As recommended by American Petroleum Institute Recommended Practice 61, a series of closure stresses are utilized ranging from 1000 psi – 6000 psi in 1000 psi intervals to test the fracture conductivity. To obtain results related to the strength of a proppant, a sieve analysis is conducted before and after fracture conductivity testing. The sieve analysis provides a grain size distribution and quantitative analysis of proppant crushing.

It was concluded from this study that limestone reacts favorably to being acid fractured at low acid residence times and yields conductivity values higher than those of a propped fracture. The results indicate that a short acid pre-flush followed by proppant maximizes the conductivity of the limestone while longer acid pre-flushes minimize conductivity as the dissolution weakens the rock's ability to support the fracture. This study offers an insight into the conductivity of limestone formations and how acid

affects the near-wellbore conductivity while presenting a detailed methodology for quantifying fracture conductivity in a laboratory setting.

DEDICATION

I would like to thank God for providing this opportunity and allowing me to see it through. I would also like to thank my family and friends for their support. Furthermore, I'd like to thank Grace Bible Church for being an awesome community and allowing me to serve in the family ministry, as well as at Junction, and for the many fun times and growth.

ACKNOWLEDGEMENTS

I would like to thank my advisor and committee chair, Dr. Dan Hill, for the opportunity to pursue my graduate degree. Dr. Dan Hill has been a mentor and has made time here interesting and a pleasure. I would also like to thank committee member Dr. Ding Zhu for providing advice and wisdom throughout my studies. Lastly, I would like to thank Dr. Art Donovan from the Department of Geology for being my out of department committee member.

I would also like to thank Edmond Obi and Tohoko Tajima for help conducting experiments. As well as Gabe Tatman and Smith Leggett for their conversations. Lastly, I'd like to thank John Maldonado for his help in the laboratory.

CONTRIBUTORS AND FUNDING SOURCES

Contributors

This study was conducted under the committee supervision of Dr. Dan Hill and Dr. Ding Zhu of the Harold Vance Department of Petroleum Engineering, as well as Dr. Art Donovan of the Department of Geology.

Technical assistance was provided by Edmond Obi and Tohoko Tajima of the Harold Vance Department of Petroleum Engineering.

All other work conducted for this thesis was completed by the student independently.

Funding Sources

Graduate study was supported by a fellowship from Texas A&M University and a Research Assistantship for the study of fracture conductivity provided by Texas A&M University and funded by the U.S. Department of Energy.

NOMENCLATURE

dP/dL	Pressure gradient across the proppant pack (psi/ft)
q	Volumetric flow rate (ft/s)
A	Cross-sectional area (in2)
w_f	Fracture width (thickness) (in)
h_f	Fracture height (width) (ft)
k_f	Fracture permeability (md)
L	Sample length (ft)
M_g	Molecular mass (kg/mol)
$\dot{M}$	Mass flow rate (kg/min)
P_1	Upstream pressure (psi)
P_2	Downstream pressure (psi)
P_{cell}	Cell pressure (psi)
R	Universal gas constant (J/mol K)
T	Temperature (K)
V	Fluid velocity (m/s)
Z	Gas compressibility factor
ρ_f	Density of fluid (kg/m3)
μ	Viscosity of fluid (cP, Pa-s)
Δp	Differential pressure (psi)
C_f	Fracture conductivity (md-ft)

TABLE OF CONTENTS

Page

ABSTRACT ii

DEDICATION v

ACKNOWLEDGEMENTS vi

CONTRIBUTORS AND FUNDING SOURCES vii

NOMENCLATURE viii

TABLE OF CONTENTS ix

LIST OF FIGURES xi

LIST OF TABLES xiv

1. INTRODUCTION AND LITERATURE REVIEW 1

1.1. Background 1
1.2. Literature Review 2
1.2.1. Hydraulic Fracturing 2
1.2.2. Fracture Conductivity 4
1.3. Objective of the Study 9

2. EXPERIMENTAL DESIGN AND METHODOLOGY 10

2.1. Introduction 10
2.2. Conductivity Sample Preparation 10
2.2.1. Sample Fracturing 10
2.2.2. Surface Laser Profile Scan 11
2.2.3. Sample Mineralogy 12
2.2.4. Proppant Sieve Analysis 13
2.2.5. Proppant Concentration Calculation 14
2.2.6. Acid Residence Time Calculation 14
2.2.7. Proppant Placement 15
2.2.8. Sample Preparation Procedure 16
2.3. Experimental Methodology and Procedure 20
2.3.1. Experiment Design 20

2.3.2. Experimental Equipment 22
2.3.3. Fracture Conductivity Calculation 24
2.3.4. Experimental Procedure 28
2.4. Design Considerations and Experimental Challenges 37
2.5. Experimental Conditions 38

3. RESULTS 40

3.1. Introduction 40
3.2. Proppant Size Analysis 40
3.2.1. Grain Size Analysis of the Proppant Only Tests 40
3.2.2. Grain Size Analysis of Acid + Proppant Tests 42
3.3. Surface Analysis 46
3.3.1. Surface Scans of Proppant Only Tests 47
3.3.2. Surface Scans of Acid and Acid + Proppant Tests 48
3.3.3. Volumetric Change Calculations 53
3.4. Conductivity Analysis 54
3.4.1. Acid Fracture Conductivity 54
3.4.2. Propped Fracture Conductivity Results 55
3.4.3. Propped Acid Fracture Conductivity Results 56
3.4.4. Combined Conductivity Results 58

4. CONCLUSIONS 61

4.1. Conclusions 61
4.2. Recommendations 62

REFERENCES 63

LIST OF FIGURES

Page

Figure 1. Proppant distribution on a rough shale fracture surface: (a) initial proppant pack, (b) proppant rearrangement during the application of closure stress, and (c) proppant crushing as the rock creeps at high closure stress (Reprinted from Zhang, 2014). 6

Figure 2. The effects of proppant embedment on the fracture aperture (Reprinted from Fernandez, 2019). 7

Figure 3. Fracture conductivity sample dimensions (Reprinted from Copeland, 2020). . 11

Figure 4: X-ray diffraction analysis results for the limestone outcrop..... 13

Figure 5: Grainsize distribution of the provided 40/70 mesh proppant. 14

Figure 6: Proppant evenly distributed onto the bottom of the sample (the sample half at the bottom of the figure). 16

Figure 7: Conductivity sample under a fume hood with primer drying on the sample (white substance on the surface of the sample). 17

Figure 8: Sample mold and mold release spray under a fume hood. 18

Figure 9: A) depicts the wing screw used to remove half of the mold and B) is the hydraulic press used to remove the sample from half of the mold. 20

Figure 10: Experimental schematic for measuring fracture conductivity. 21

Figure 11: Experimental setup in the laboratory. 22

Figure 12: Pressure port schematic of pressures measured from the front of the test cell..... 26

Figure 13: Experimental results to determine fracture conductivity (modified from Wylie, 2018). 28

Figure 14: GCTS Computer Aided Testing System screen layout. 29

Figure 15: Picture of a sample prepared for loading into the test cell..... 30

Figure 16: Test cell and pistons wrapped in Teflon sealant tape and bracket. 31

Figure 17: Experimental setup showing the gas cylinders and flow gauges. 34

Figure 18: Sieve analysis of smooth cut sample proppant only. 41

Figure 19: Sieve analysis of fractured sample proppant only. 41

Figure 20: Sieve analysis of 10-minute residence time propped sample. 42

Figure 21: Sieve analysis of 20-minute residence time propped sample Test 1. 43

Figure 22: Sieve analysis of 20-minute residence time propped sample Test 2. 44

Figure 23: Sieve analysis of 1.5-minute residence time propped sample Test 1. 45

Figure 24: Sieve analysis of 1.5-minute residence time propped sample Test 2. 45

Figure 25: Pictures of test samples after conductivity testing with a) the smooth cut proppant only test b) the 10-minute residence time propped sample c) the first 20-minute residence time propped sample and d) the second 20-minute residence time propped test. 46

Figure 26: Post-test scans of smooth cut surface after conductivity testing. 47

Figure 27: Post-test scans of the fractured surface after conductivity testing. 48

Figure 28: Post-test scans of the 10-minute residence time acid fracture. 49

Figure 29: Post-test scans of the 10-minute residence time propped acid fracture. 49

Figure 30: Post-test scans of the 20-minute residence time propped acid fracture Test 1. 50

Figure 31: Post-test scans of the 20-minute residence time propped acid fracture Test 2. 51

Figure 32: Post-test scans of the 1.5-minute residence time propped acid fracture Test 1. 52

Figure 33: Post-test scans of the 1.5-minute residence time propped acid fracture Test 2. 52

Figure 34: Calculated acid fracture conductivity values for limestone outcrop with 15% hydrochloric acid with a 10-minute residence time. 55

Figure 35: Calculated conductivity values for limestone outcrop with 0.2 lb/ft^2 40/70 mesh. 56

Figure 36: Calculated conductivity values for acid fractured samples with 0.2 lb/ft2 40/70 mesh proppant.....58

Figure 37: Combined calculated conductivity values from all tests performed.....60

LIST OF TABLES

Page

Table 1: Fracture conductivity experimental conditions. 39

Table 2: Volume change calculation results from MATLAB code. 53

1. INTRODUCTION AND LITERATURE REVIEW

1.1. Background

Oil and gas production from conventional reservoirs, described as consisting of mostly sandstones or carbonates with relatively high permeability and porosity, has led to a depletion of reserves from these reservoirs in the United States. In order to continue to supply the world with oil, the source rocks that provide hydrocarbons to conventional reservoirs and extremely tight reservoir formations are being explored and developed due to technological advancements. These reservoirs, typically called unconventional reservoirs, are very fine-grained clastic sedimentary or carbonate rocks that have relatively very low permeability and porosity.

The primary method to stimulate tight reservoirs for better productivity is hydraulic fracturing. This method increases contact area with the reservoir and allows hydrocarbons to migrate to the wellbore. There are two methods to hydraulically fracture a formation. One way is to pump viscous or non-viscous proppant loaded fluid into the formation at pressures above the formation's fracture gradient. Proppant helps prevent the generated fractures from closing and allows hydrocarbons to flow through conductive channels to the wellbore. The other method is to pump acid above the fracture gradient into the formation. Acid etched high points and incongruent surfaces act to support the fracture in place of proppant.

An important parameter when evaluating and predicting the success of a fracture is fracture conductivity. Researchers have developed, modified, and improved laboratory procedures to quantify fracture conductivity, which is mathematically described as a

fracture's width times the permeability of the proppant pack or acid etched fracture (Cooke, 1973). Many have used this definition to explain how well hydrocarbons flow through the fracture. Higher conductivities indicate that the fluid flows better through the medium. To compare the efficacy of fracture designs with one another, dimensionless fracture conductivity is used. It is the ratio of the fracture's ability to transport fluid through the fracture over the reservoir's ability to transport fluid to the fracture (Larsen et al, 1985).

The necessity of hydraulic fracturing to produce unconventional reservoirs has led to a variety of conductivity tests being performed on downhole core and outcrop samples from many formations, with a variety of proppants of varying material and size being tested with the goal of enhancing fracture performance. The following work presented in this thesis is a continuation of that investigation with a specific focus on limestone formations.

1.2. Literature Review

There have been several studies analyzing hydraulic fracturing improvements through the quantification of fracture conductivity in laboratories. This section provides a review of some of these studies.

1.2.1. Hydraulic Fracturing

The first hydraulic fracturing treatment occurred in 1947 at the Hugoton gas field in Kansas by Stanolind Oil with a procedure called hydrafrac (Clark, 1949). Hydraulic fracturing is a stimulation process in which a hydraulic fluid is pumped into a wellbore at a pressure that exceeds the fracture gradient of the formation, creating artificially

made fractures that increase reservoir contact area and thus increases the amount of production from a well. While the fundamental principles are the same, hydraulic fracturing today is very different from its origins. Instead of using highly viscous fluids and creating large and short fractures, less viscous fluids such as slickwater are used today with different amounts and sizes of proppant to generate longer skinnier fractures. Various solids have been tested as proppants.

Engineers and researchers are continuing to improve and optimize proppant application and hydraulic fracturing techniques as it is vital to produce hydrocarbons from tight reservoirs (Almubarak et al, 2020). The design of hydraulic fracture treatments varies by operator and field, but common practice today is to use slickwater, a mixture of water and friction reducers, for propped fractures and hydrochloric acid for acid fractures (Almubarak et al, 2020). An important mechanism to consider during the design process is proppant transport. Low viscosity fluids have little ability to suspend and transport proppant. Higher injection rates, smaller proppant sizes, and smaller proppant concentrations are all actions that have been taken to counteract the poor ability of slickwater to transport proppant and improve overall fracture performance (Palisch et al, 2010).

Acid fracturing is another type of hydraulic fracturing where acid etched surfaces support the fracture and hold it open under closure stress. Instead of slickwater, a viscous fluid and an acid are pumped into the formation above the fracture gradient to create the fracture and dissolve the fracture face. This practice is used in carbonate

formations. Significant experimental work has been conducted to test different acid systems and their impact on fracture conductivity (Jin, 2020).

1.2.2. Fracture Conductivity

C. E. Cooke (1973) performed significant research on fracture conductivity in the 1970s, looking at how fluid type, temperature, and flow rate impacted a proppant's conductivity. Fracture conductivity is defined as the product of the proppant pack permeability multiplied by fracture width (Cooke, 1973). Fracture conductivity is used to measure the quality of the stimulation and is representative of the fracture's ability to allow fluid to flow through the fracture. Dimensionless fracture conductivity is the ratio of fracture conductivity and the product of reservoir permeability multiplied by fracture half length, or the reservoirs ability to allow fluid to flow. Proppant variables such as size, type, shape, and quantity alter conductivity as they change a fluid's ability to flow through the proppant pack.

Determining the properties and characteristics of proppant provides an understanding of how the proppant behaves in the fracture under high stress conditions. The ideal fracture treatment should have a proppant that consists of large, spherical, uniformly-sized particles that have a strength that can withstand the overburden and closure stresses of the formation. D. G. Larsen and L. J. Smith (1985) concluded that proppant sphericity, the degree the proppant resembled a sphere, and roundness, how smooth the proppant is, impacts the conductivity and permeability of the proppant pack both positively and negatively (Larsen et al, 1985). As grains become more spherical,

the pore space between them increases and subsequently the permeability increases, increasing fracture conductivity.

Since the late 1980s, Stim-Lab has been conducting experiments on proppants to determine their conductivity and analyze the impact the various design parameters such as the type of proppant and the concentration, fluid type, fluid flow rate, temperature, as well as cyclic loading (Duenckel et al, 2017). Through numerous tests, they found how each design parameter impacted the conductivity of the proppant pack to provide insight into completions designs with the goal of improving conductivity and predicting conductivity in simulations and modelling (Duenckel et al, 2017).

A selected proppant must be able to withstand the closure stress of the formation because if it cannot, proppant crushing occurs which negatively impacts fracture conductivity. **Figure 1** illustrates the stages of crushing a proppant may undergo as closure stress is applied to the fracture surface (Zhang, 2014). Fracture conductivity reduces during proppant crushing as the proppant grain sizes become smaller and fracture width decreases. This results in a decrease in permeability as proppant and reservoir pore spaces clog up from the resulting fines (Cooke, 1977).

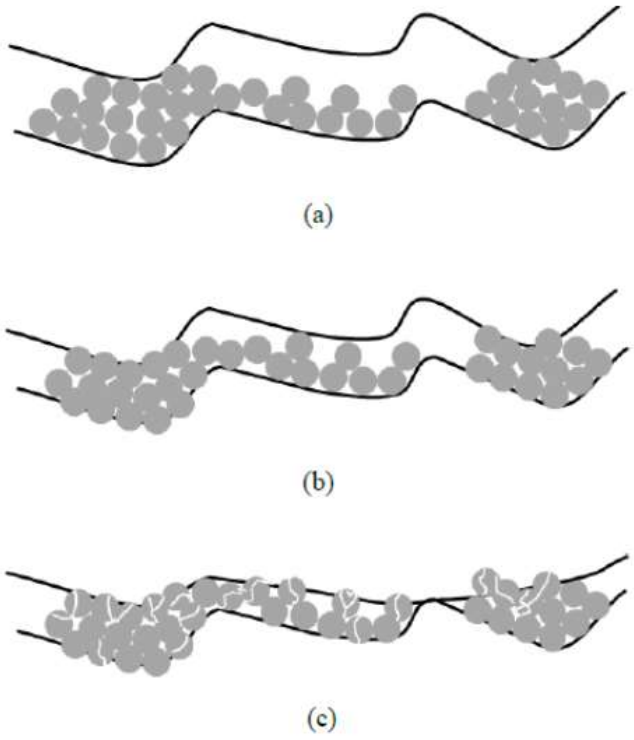

Figure 1. Proppant distribution on a rough shale fracture surface: (a) initial proppant pack, (b) proppant rearrangement during the application of closure stress, and (c) proppant crushing as the rock creeps at high closure stress (Reprinted from Zhang, 2014).

Another negative impact on fracture conductivity is proppant embedment. As the fracture closes, proppant may become embedded onto the fracture surface, reducing the fracture's aperture. The Young's Modulus as well as mineralogical properties of the formation play an important role on the amount of embedment that occurs. As the Young's Modulus of the formation decreases, the amount of embedment increases (Fernandez, 2019). **Figure 2** illustrates the effect of embedment. The type of fluid used during fracturing and proppant delivery greatly impacts proppant embedment with liquids causing more embedment as they soften the fracture surface (Winner, 2018).

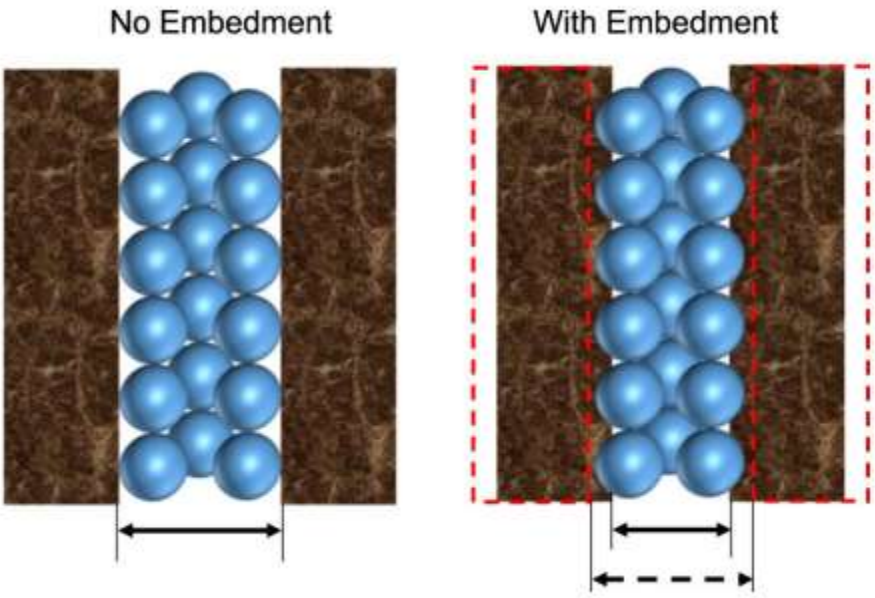

Figure 2. The effects of proppant embedment on the fracture aperture (Reprinted from Fernandez, 2019).

Fracture conductivity tests performed in the laboratory used a modified American Petroleum Institute test cell as described in the American Petroleum Institute Recommended Practice 61. The modified cell allows for the testing of larger samples while maintaining pressure. These procedures allowed for more realistic testing conditions. While dry nitrogen was used for these tests as it does not change the integrity of the shales, dry gas, wet gas, brine, oil, and multiphase fluids may be used as well as a variety of proppant loads and acid etched fracture surfaces (Zhang, 2014).

High degrees of complexity and heterogeneity play a significant role in acid fracturing as it impacts etching pattern, etching volume, and the aperture which determines the acid fracture conductivity. Instead of relying on proppant to hold the

fracture open, acid fractures rely on high points in the etching pattern to support the fracture.

In 2007 M. Melendez studied acid contact time with respect to creating conductivity in acid fractures. Melendez found that acid fracture conductivity is governed by the etching pattern of the rock surface and is influenced by the rock hardness. She concluded that longer residence times didn't always correspond to higher conductivities, but that higher conductivities were associated with channels dissolved in the rock surface. If dissolved channels were not created, rock hardness became the dominating factor determining conductivity (Melendez, 2007). Melendez provided a methodology to perform an acid fracture on carbonate samples and to analyze the dissolved pattern using 3 dimensional scans.

Petrobras looked into characterizing acid etched patterns in 2012 to better simulate fracture surfaces in the field. They concluded that work up until 2012 focused on using samples that were flat while fractures in the field were naturally rough. Their study supported Nierode and Kruk who found in 1973 that acid smooths the surfaces of tensile fractures (Neumann et al, 2012). Furthermore, it was found that acid conductivity is generated from surfaces that are mismatched with one another (Neumann et al, 2012).

X. Wang in 2015 compared the conductivity of acid fractures with the conductivity of both propped and unpropped fractures. Wang found that propped conductivity was higher than acid conductivity at high closure stresses and found that under low closure stress, fracture surface channels improved the conductivity of the acid fracture surfaces (Wang, 2015). Acid fracture conductivity was improved if the rock had

higher percentages of dolomite which would increase the rocks ability to support the acid fracture (Wang, 2015).

1.3. Objective of the Study

The objective of this study is to evaluate acid fracture conductivity versus propped conductivity in limestones to optimize fracture design. This study has a further objective to evaluate an integrated design of acid plus proppant.

2. EXPERIMENTAL DESIGN AND METHODOLOGY

2.1. Introduction

This section outlines how the samples were prepared for the fracture conductivity tests as well as the procedures and equipment used. Some of the procedures applied are comparable to previous work performed by Zhang (2014), Wylie (2018), Winner (2018), Guerra (2019), Fernandez (2019), and Copeland (2020). Limestone rock outcrop samples were purchased from Kocurek Industries who sourced the outcrop from an Austin, Texas area quarry.

Six limestone outcrop samples were tested. Two tests were performed with a 40/70 mesh proppant provided by SM Energy. One test was performed with 15% hydrochloric acid with a 10-minute residence time. Three tests were performed on outcrop samples that were acid fractured with 15% hydrochloric acid and then packed with the 40/70 mesh proppant.

2.2. Conductivity Sample Preparation

This section discusses the preparation of the samples used for conductivity testing.

2.2.1. Sample Fracturing

Kocurek Industries cut and fractured all samples into the dimensions required to securely fit in the Modified American Petroleum Institute conductivity cell. Berea sandstone spacers glued to the top and bottom of the sample ensure each sample fits evenly inside the test cell. The spacers also allowed the fracture to align with the sensor

ports as well as the inlet and outlet nitrogen flow lines located on the test cell. **Figure 4** shows the dimensions of the conductivity sample.

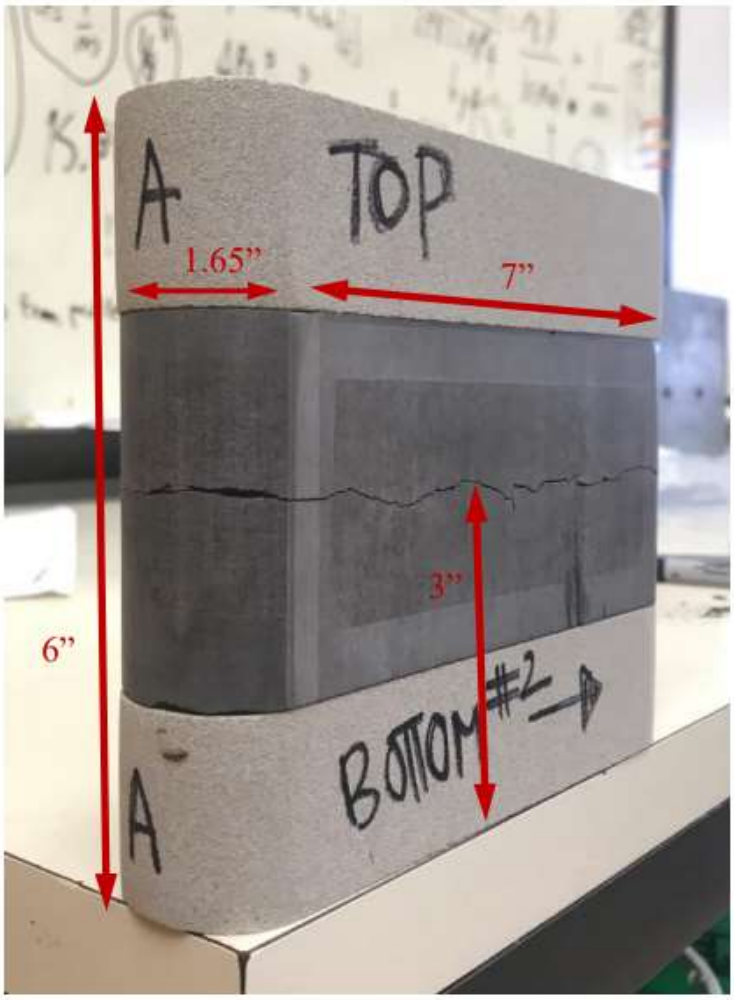

Figure 3. Fracture conductivity sample dimensions (Reprinted from Copeland, 2020).

2.2.2. Surface Laser Profile Scan

Prior to preparation, the sample halves were labeled top and bottom and the direction of flow through the fracture was determined while keeping in mind the fracture needed to be in line with the test cell ports. Once the direction of flow was determined, a

laser profilometer scanned the fracture surface before conductivity preparation and testing as well as after testing to analyze changes in the surface. Jin (2020) presented the procedure and equipment used to scan the sample. The laser profilometer moves the sample in the x- and y-directions taking a measurement of the height of the sample, the z-direction, at a single point (Jin, 2020). The profilometer software outputs a text file with the x, y, and z measurements. A MATLAB program converts and plots a 3-dimensional fracture surface profile.

Comparing the surfaces of the sample with the conductivity results allowed for a better understanding of what influenced the calculated conductivities with an emphasis on identifying if proppant embedment had occurred. Fracture conductivity reduces as proppant crushes due to fines migration and embedment (Cooke, 1977). Pore throats become blocked as embedment occurs which decreases flow from the reservoir. Calculated fracture surface volume changes help explain how proppant crushing and embedment negatively impact fracture conductivity. For the acid conductivity samples, these scans provided a way to identify how the fracture and sample withstood the applied closure stress.

2.2.3. Sample Mineralogy

An X-Ray Diffraction test was performed on the outcrop to determine the mineralogy of the rock sample. The limestone outcrop sample is mostly comprised of calcite with a small percentage of quartz. The results are presented in **Figure 5** below.

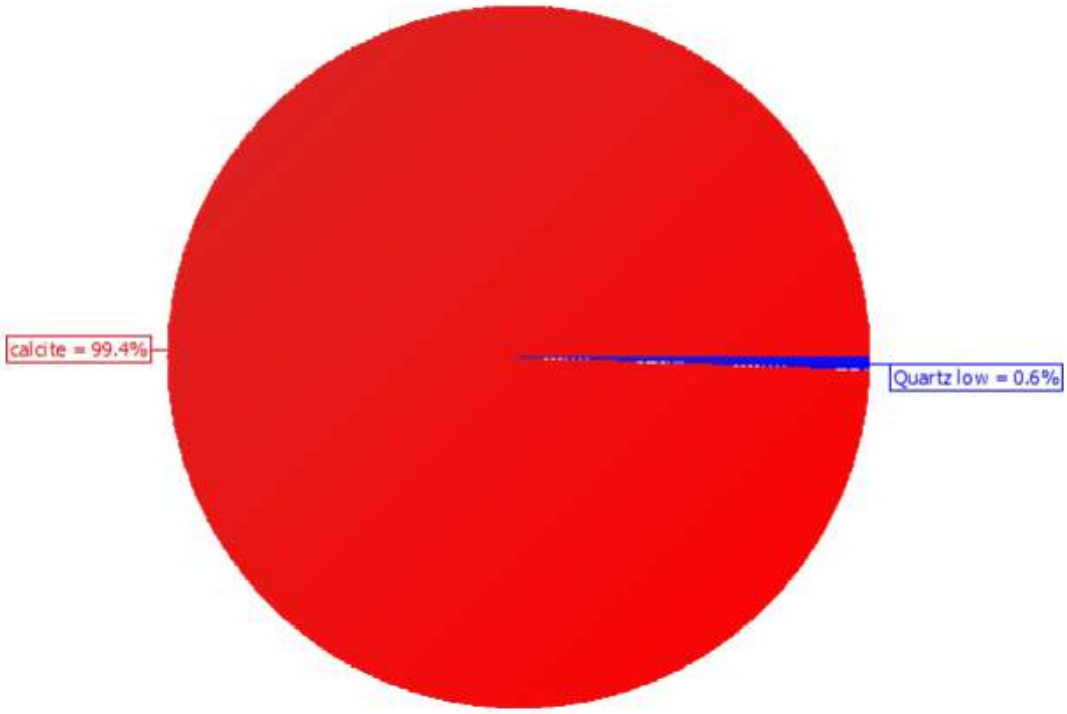

Figure 4: X-ray diffraction analysis results for the limestone outcrop.

2.2.4. Proppant Sieve Analysis

Five samples using the limestone outcrop were made with 40/70 mesh proppant provided by SM Energy. **Figure 5** presents a sieve analysis of the provided 40/70 mesh proppant using the American Society for Testing and Materials standards to find the grain size distribution (ASTM, 2019). Typical 40/70 mesh proppants have grains that are smaller than a No. 40 sieve and larger than a No. 70 sieve. Appendix A presents the results of all the sieve analyses.

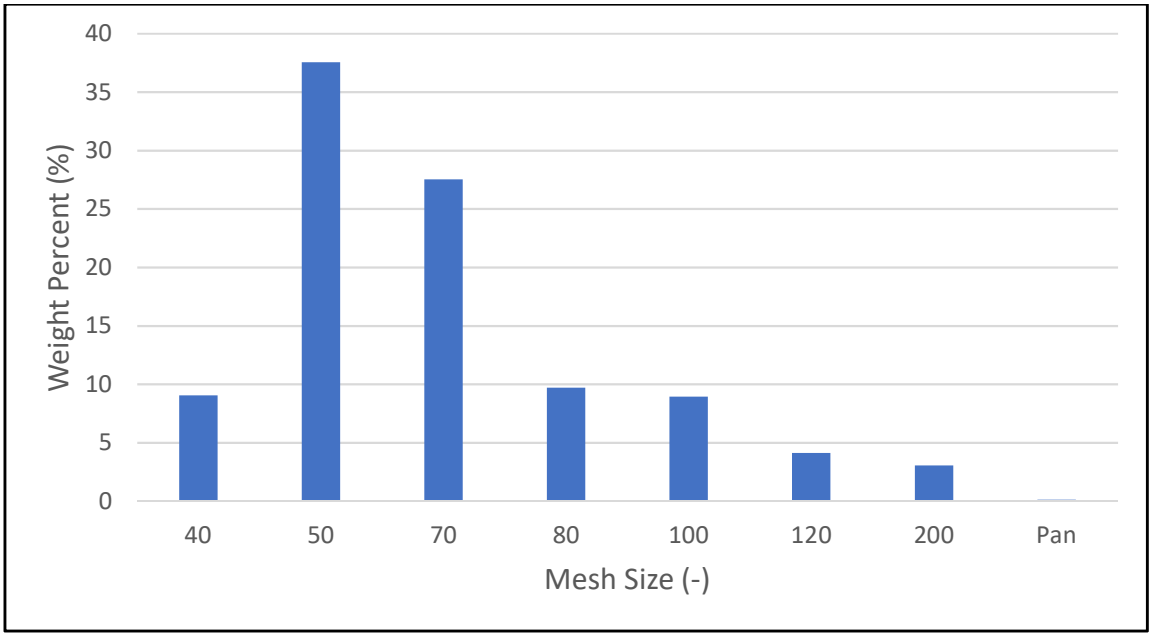

Figure 5: Grainsize distribution of the provided 40/70 mesh proppant.

2.2.5. Proppant Concentration Calculation

For the five tests that used proppant, a concentration of 0.2 lb_m/ft^2 was used. The same mass of proppant was measured for each propped sample to maintain consistency. The mass of the proppant that reflected 0.2 lb_m/ft^2 was found using the same methodology as Winner (2018) and Copeland (2020). Assuming a planar fracture area, the total fracture surface area of the samples was found to be 0.0762 ft^2 and the corresponding mass of the proppant required was 6.81 g.

2.2.6. Acid Residence Time Calculation

Acid fracture residence time it the amount of time live acid is in the fracture. The more time the acid spends inside the fracture, the more the formation will be dissolved. Residence time is calculated by dividing the total volume of the fluid pumped by the flowrate of the fluid pumped. An acid pre-flush design of 2000 gallons of acid pumped

at 30 bbls/min was used to determine a 1.5-minute residence time. 10- and 20-minute residence times were also used as they are standard residence times for acid fracture conductivity comparison.

2.2.7. Proppant Placement

After the surface scans, proppant is evenly distributed onto the sample's bottom fracture surface as shown in **Figure 6**. Performing this process over a clean piece of white paper ensures that all the grains measured out were spread onto the fracture surface by providing a way to capture any grains that fall off the fracture surface. Once the grains are evenly distributed, the top of the sample is placed onto the bottom and the fracture sealed off with super glue and tape. The rest of the sample is epoxied and loaded into the Modified American Petroleum Institute test cell as described in the following procedures.

Figure 6: Proppant evenly distributed onto the bottom of the sample (the sample half at the bottom of the figure).

2.2.8. Sample Preparation Procedure

1) Place the bottom of the sample on a clean sheet of paper.
2) Evenly distribute the measured proppant to the required mass to meet the desired concentration.
3) Place the top of the sample onto the bottom of the sample, being sure to carefully align both halves. From here on out, be extremely careful with the sample. Be sure not to jostle the sample, keeping it straight and upright.

4) Apply two lines of gelled superglue, one above the fracture and one below, and tightly glue painter's tape around the fracture to prevent epoxy from leaking into the fracture.
5) Use steel wool to smooth the tape down and remove air bubbles and creases in the tape. The tape must be smooth otherwise air pockets may form that allow for nitrogen to flow around the test sample instead of through the fracture.
6) Under a fume hood, apply a coat of Momentive SS4155 01P primer to the sample (**Figure 7)**. Allow the primer to dry for 15 minutes.

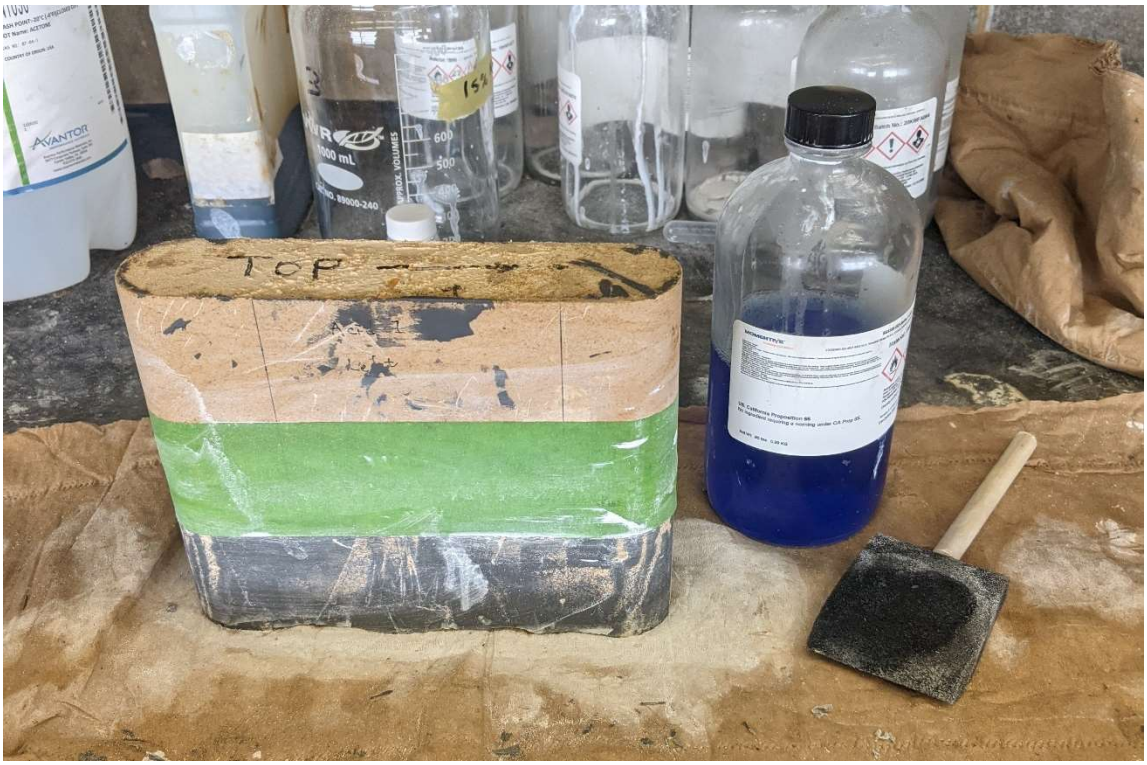

Figure 7: Conductivity sample under a fume hood with primer drying on the sample (white substance on the surface of the sample).

7) Repeat Step 6 two more times for a total of 3 coats of primer.

8) While the primer dries, clean the surfaces of the mold that touch the sample with acetone.

9) Once clean, apply a generous coat of CRC Food Grade Mold Release to the surfaces of the mold that touch the sample under a fume hood (**Figure 8)**. Allow 5 minutes for the mold release to dry.

Figure 8: Sample mold and mold release spray under a fume hood.

10) Repeat Step 9 two more times for a total of 3 coats of mold release.
11) Apply high pressure vacuum grease to the surfaces of the mold where the mold comes together. Tightly screw the mold together.
12) Gently place the primed sample into the assembled mold. Be extremely careful not to jostle the sample, but hold it upright to maintain the evenly distributed proppant.
13) Mix the two components of Momentive RTV627 022 epoxy using a 50:50 ratio, that is 50 grams of Part A and 50 grams of Part B. Mix the epoxy thoroughly and allow 5 minutes for trapped air bubbles to rise to the surface.
14) Using a 60 mL syringe, slowly pour the epoxy into the void space between the sample and the mold.
15) Once the epoxy reaches the edge of the mold, allow 5 minutes for trapped air bubbles to rise to the surface.
16) After allowing trapped air bubbles to rise, place the mold into an oven to cure for 2 hours at a temperature of 165° F (dial number 4 on the Quincy Lab Oven 10GC).
17) After 2 hours, remove the mold from the oven and carefully remove the sample from the mold using the wing screw as seen in **Figure 9 (A)** to remove on side of the mold and using the hydraulic press in **Figure 9 (B)** to press the sample off the

second half of the mold.

Figure 9: A) depicts the wing screw used to remove half of the mold and B) is the hydraulic press used to remove the sample from half of the mold.

18) Repeat Steps 6 – 17 for the top half of the sample. Use sandstone spacers to support the mold brackets around the sample.

2.3. Experimental Methodology and Procedure

This section explains the experimental design, equipment, and procedure for fracture conductivity testing.

2.3.1. Experiment Design

The system utilized to quantify fracture conductivity included the following components:

1) Modified American Petroleum Institute fracture conductivity cell.
2) GCTS hydraulic load frame.
3) Nitrogen gas reservoir contained in a pressurized dry nitrogen cylinder.
4) Cell and differential pressure transducers.

5) Gas flowmeter.

6) Backpressure regulator.

7) GCTS Testing Systems control system connected to a PC containing a data acquisition software.

Figure 10 shows a schematic of the system.

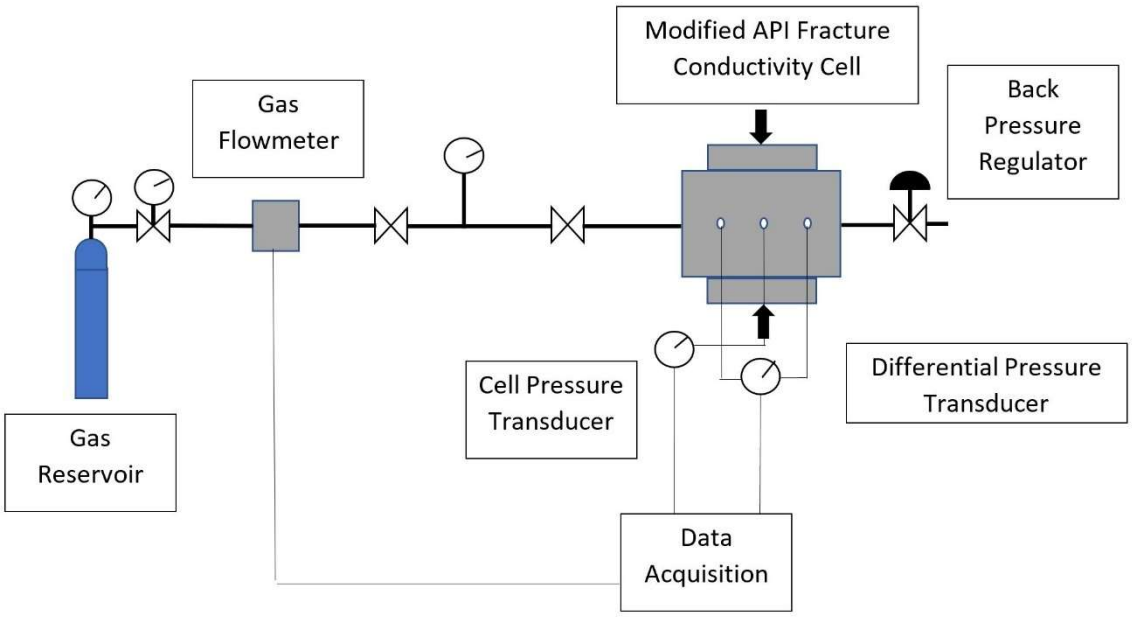

Figure 10: Experimental schematic for measuring fracture conductivity.

The test samples are carefully placed inside the test cell and a load applied to the top piston inserted into the top of the cell. The samples were loaded to 1000 psi, 2000 psi, 3000 psi, 4000 psi, 5000 psi, and 6000 psi closure stresses. Nitrogen was flowed through ¼ inch flow lines from the nitrogen gas cylinder into the Modified American Petroleum Institute fracture conductivity cell and through the fracture while the gas flowmeter measured the flowrate. The pressure transducers measured the cell and

differential pressure inside the test cell and displayed them on the GCTS Testing Systems Computer Aided Testing System software on the PC throughout the experiment. A backpressure regulator controls the flow exiting the cell. **Figure 11** depicts the experiment setup used in the laboratory. Section 2.3.4 provides test procedures.

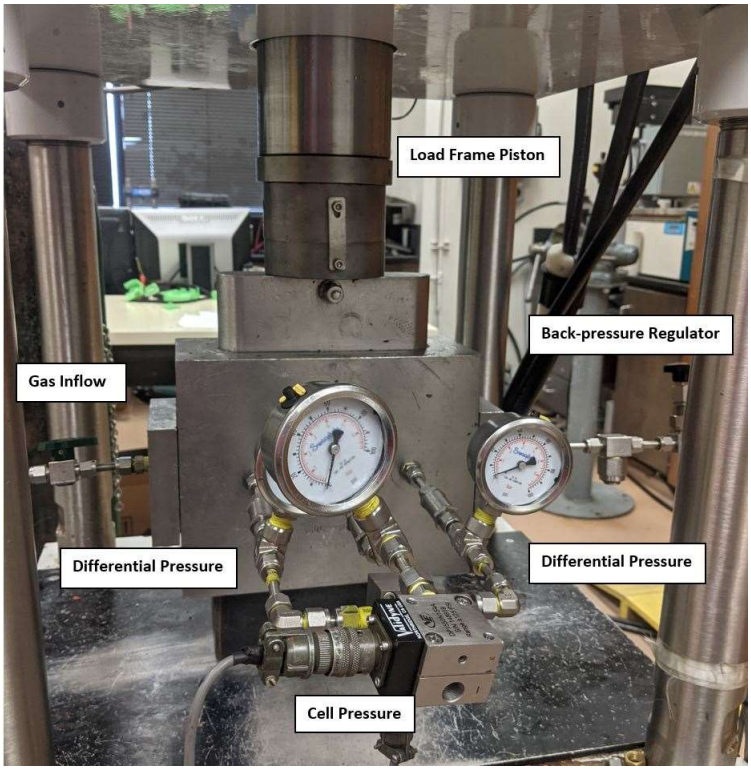

Figure 11: Experimental setup in the laboratory.

2.3.2. Experimental Equipment

The set-up used for this study was developed and modified by Kamenov (2013), Zhang (2014), and Guerra (2019) with each component notated in **Figure 11**. The GCTS Testing System load frame was a GCTS FRM4-1000-50s with a loading capacity of

208,000 lb_f and a maximum loading rate of 1,215 lb_f/min. A control box linked to a computer with a data acquisition system controls the hydraulic pump driving the load frame. The software outputs the closure stress applied to the sample, the axial displacement of the load frame piston, the cell pressure, and the differential pressure experienced across the fracture. These outputs are used to calculate the fracture conductivity inside the Modified American Petroleum Institute test cell.

The test cell securely holds the sample in place during testing and has three ports located on the front of the cell for the cell pressure and differential pressure transducers. Slots that are ¼ inch by ¼ inch are cut into the epoxied sample to allow flow through the pressure transducer lines. The dimensions of the cell are 10 inches in length, 4 inches in width, and 8 inches in height. Dimensions for the inner cavity were 7 inches in length, 1 inch in width, and 8 inches in height with circular ends with a radius of 0.8785 inches.

Dimensions for the pistons used to apply pressure onto the sample are 7 inches in length, 1 inch in width, and 3 inches in height. The pistons need to be secured inside the cell to distribute the load of the hydraulic load frame onto the sample and align with the sample inside the cell, asserted above and below the sample. A tubular conduit connects the base of the piston with a relief valve on the outside of the piston. This allows for the installation of leak off lines if needed and aids in the removal of the top piston after the experiment is complete. For all tests, the bottom relief valve was sealed. O-rings surround the pistons and cell endcaps to further prevent nitrogen leak off from the cell.

An Aalborg GFC Mass Flow Controller measures the mass flowrate of the nitrogen injected into the test cell from a gas reservoir. The capacity of the flowmeter

was 10 L/min. The manufacturer calibrated the flowmeter to nitrogen gas. The accuracy of the measurement was ± 1% of the full-scale flowrate which is ± 0.1 L/min (Guerra, 2019).

A Validyne Model DP15 50N1S4A transducer with a 3-50 diaphragm that has a pressure threshold of ± 125 psi measured cell pressure and a Validyne Model DP15-32 transducer with a 3-32F diaphragm that has a pressure threshold of ± 2 psi measured differential pressure. The back-pressure regulator valve controlled flow to increase or decrease the cell and differential pressures once the cell pressure reached 30 psi. A Swagelok needle valve connected to an outlet flow line was the back-pressure regulator. Twisting the valve allowed nitrogen to flow out of the cell while being carefully manipulated.

2.3.3. Fracture Conductivity Calculation

The Darcy equation (**Eq. 1)** was used to derive the equation for calculating fracture conductivity,

$$-\frac{dP}{dL} = \frac{\mu v}{k_f} \tag{1}$$

where $-\frac{dP}{dL}$ is the pressure drop over a unit length, μ is fluid viscosity (cP), v is fluid flow velocity, and k_f is fracture permeability (md). Winner (2018) found that the Darcy Law derivation could be used for flowrates under 2 L/min with a proppant concentration of 0.1 lb_m/ft^2 and Copeland (2020) found that the Darcy Law derivation could be used with a proppant concentration 0.2 lb_m/ft^2. A proppant concentration of 0.2 lb_m/ft^2 was used for all propped samples and flow rates did not exceed 2 L/min.

To begin the derivation, **Eq. 1** is multiplied by the fluid density pumped through the fracture, ρ_f, as the first step in removing the unknown velocity variable from the equation.

$$-\frac{dP}{dL}\rho_f = \frac{\mu v}{k_f}\rho_f \tag{2}$$

Nitrogen was the fluid used during experiments, so the real gas law, **Eq. 3**, could applies.

$$\rho_f = \frac{PM_g}{ZRT} \tag{3}$$

Where P is pressure, M_g is the molecular weight (kg/mol), Z is the gas compressibility factor, R is the universal gas constant (J/mol-K), and T is the temperature (K). To eliminate unknowns in **Eq. 3**, **Eq. 4** is used to introduce measurable values as pressures and flowrates are more realistically quantified than permeabilities.

$$\rho_f = \frac{\dot{m}}{Av} \tag{4}$$

Where $\dot{m}$ is mass flow flowrate and A is flow area. Combining **Eq. 1, Eq. 2,** and **Eq. 3** forms **Eq. 5** which is integrated to get **Eq. 6**.

$$-\frac{PM_g}{ZRT}dP = \frac{\mu \dot{M}}{k_f A}dL \tag{5}$$

$$\frac{(P_1^2 - P_2^2)}{2}\frac{M_g}{ZRT} = \frac{\mu \dot{M}}{k_f A}L \tag{6}$$

Where P_1 is the upstream pressure in the test cell, P_2 is the downstream pressure in the test cell, and L is the flow path length. When determining P_1 and P_2 in the fracture, cell

pressure and differential pressure must be considered. Both are measured through pressure ports on the Modified American Petroleum Institute test cell (**Figure 12)**.

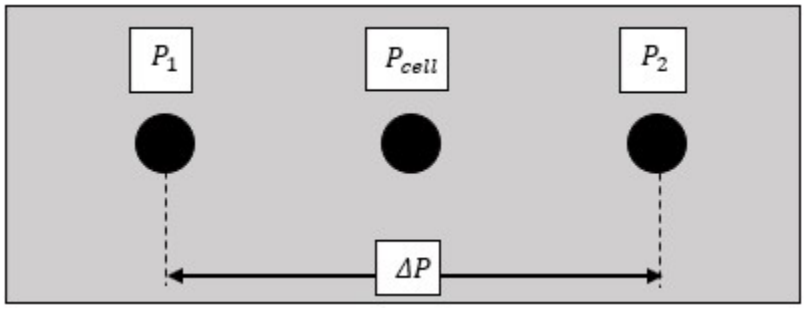

Figure 12: Pressure port schematic of pressures measured from the front of the test cell.

Figure 12 shows the cell pressure, P_{cell}, and the differential pressure, ΔP, ports where measurements are recorded. As the two differential pressure ports are an equal distance from the center cell pressure port, $(P_1\text{-}P_2)^2$ may be expressed as:

$$(P_1^2 - P_2^2) = (P_1 - P_2)(P_1 + P_2) \quad (7)$$

Where $(P_1 - P_2)$ is ΔP and $(P_1 + P_2)$ is $2P_{Cell}$. The remaining known and unknown parameters needed to calculate the fracture area (**Eq. 9**) and mass flowrate (**Eq. 10**) were substituted into **Eq. 6** to create **Eq. 11**.

$$A = w_f h_f \quad (9)$$

$$\dot{m} = q\rho_f \quad (10)$$

Where w_f is fracture width, h_f is fracture height, and q is volumetric flowrate.

$$\frac{2\Delta P P_{Cell}}{2L}\frac{M_g}{ZRT} = \frac{\mu q \rho_f}{h_f}\frac{1}{w_f k_f} \quad (11)$$

The definition of fracture conductivity, C_f, is the product of fracture width times fracture permeability. Both values are unknown and simplifying **Eq. 11** by inserting fracture conductivity leads to **Eq. 12**.

$$\frac{\Delta PP_{Cell}}{L}\frac{M_g}{ZRT} = \frac{\mu q \rho_f}{h_f}\frac{1}{C_f} \tag{12}$$

The length, L, is the length between the differential pressure ports and fracture height, h_f, is the width of the sample. The remaining unknown is C_f. Fracture conductivity is determined by plotting $\frac{\Delta P_{Cell}}{L}\frac{M_g}{ZRT}$ versus $\frac{\mu q \rho_f}{h_f}$. Using the Darcy method, as seen below in **Figure 13**, the inverse of the slope yields fracture conductivity.

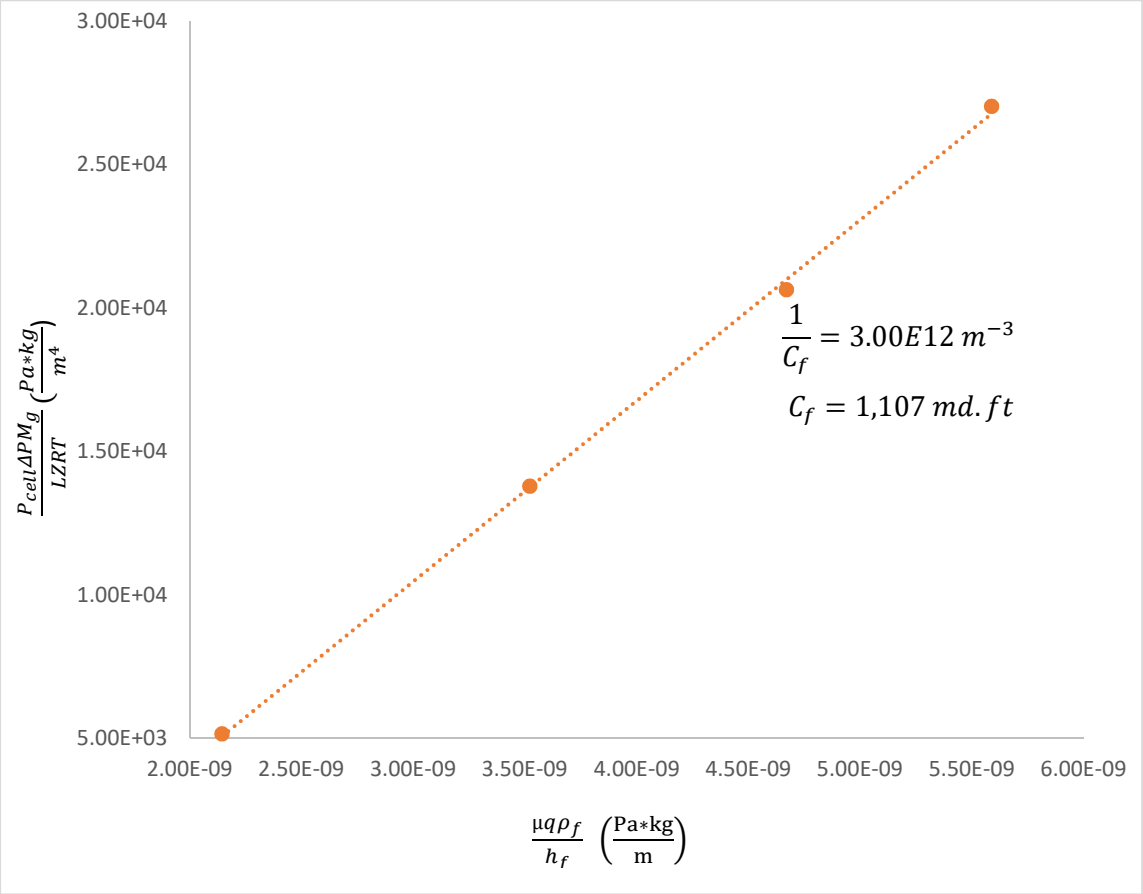

Figure 13: Experimental results to determine fracture conductivity (modified from Wylie, 2018).

2.3.4. Experimental Procedure

2.3.4.1. Fracture Conductivity Procedure

These steps were implemented in the laboratory to measure fracture conductivity for propped and acid fractured samples. Each step was performed very carefully to ensure the proppant remained undisturbed in the fracture. The cell and differential pressure transducers were calibrated prior to the start of each test. The fracture conductivity procedures are as follows:

1) Turn on the GCTS Testing Systems control box.

2) Log onto the laboratory PC and open GCTS Testing Systems Computer Aided Testing System software and load a screen layout. In the System drop down menu, select Configuration and Synchronize **Figure 14**.

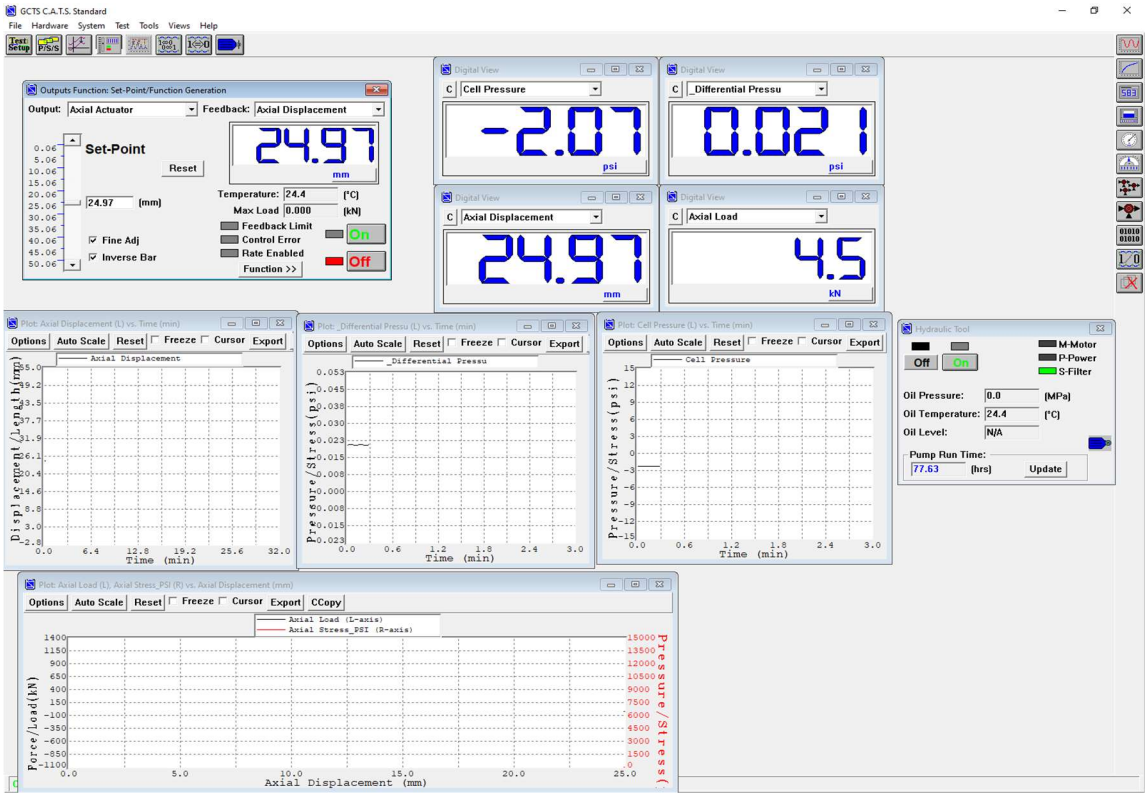

Figure 14: GCTS Computer Aided Testing System screen layout.

3) Plug the flowmeter power cable into the flowmeter.

4) Using a ruler, mark and cut the locations on the test sample where the pressure ports and flowlines are located during testing.

5) Put a thin layer of grease around the sample to act as glue for the Teflon Sealant tape at the locations seen in **Figure 15**. Stretch out Teflon Sealant tape and wrap a single layer of tape around the sample at the positions seen in **Figure 15.**

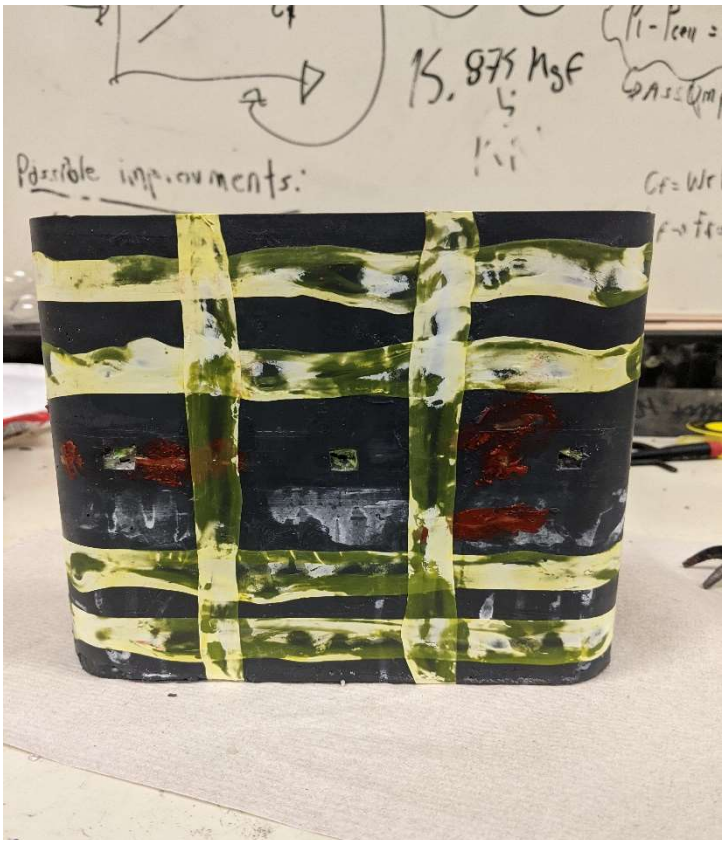

Figure 15: Picture of a sample prepared for loading into the test cell.

6) Apply a thin layer of grease all over the sample except for around the ports cut out into the front and sides of the sample.
7) Wrap three layers of Teflon Sealant tape around the O-ring on the top and bottom pistons. Make sure the bracket is around the bottom piston as seen in **Figure 16.**

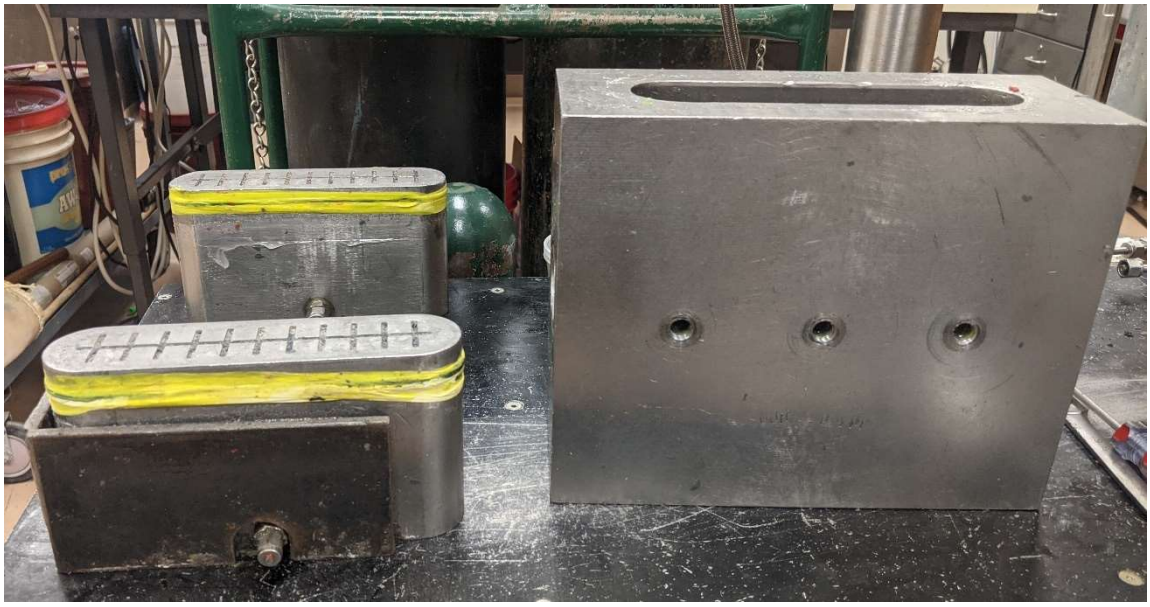

Figure 16: Test cell and pistons wrapped in Teflon sealant tape and bracket.

8) Load the bottom piston into the bottom of the test cell by pressing the piston into the opening of the test cell.
9) Load the sample into the test cell from the top by carefully pushing the sample down by hand at first and then by using the hand operated hydraulic press.
10) Load the top piston into the top of the test cell with the port on the top. Make sure that the relief nut is tight so that no air escapes.
11) Wrap a single layer of Teflon Sealant tape around one side of the double male adaptor. Insert mesh screens into the ports on the test cell and then screw the male adaptors into the ports.
12) With Teflon Sealant tape, tape a mesh screen into the opening of the inlet and outlet flow ports. Wrap three layers of Teflon Sealant tape

around the O-ring on the inlet and outlet flow ports. Insert the flow ports into the test cell and screw tight.

13) Align the test cell under the load frame so that the press is centered on the test cell.
14) On the GCTS Testing Systems Computer Aided Testing Systems Software, turn the hydraulic pump on and activate the press. Apply 15 kN, or 500 psi, to the test cell and make sure all screws and nuts are tight.
15) Make sure the nitrogen flow regulator located on the gas cylinder is closed (the screw should be all the way out) and make sure the cylinder is closed.
16) Attach the inlet line and the back-pressure regulator to the test cell making sure they are tight.
17) Before attaching the pressure sensors, calibrate the sensors using a pressure calibrator and the GCTS Testing Systems Computer Aided Testing Systems Software by going to System, Input, Analog, select either Cell Pressure or Differential Pressure, Calibrate, 2-Point Calibration. Calibrate the sensor at two different pressure points and verify that the sensor is calibrated. Once the sensors are calibrated, attach them to the test cell making sure they are tight.
18) Create a new project by clicking on the Projects Icon. Select the project and click the right arrow. Enter the sample information and

advance through the project by clicking the right arrow being sure to enter relevant information. When asked which test to run, select the desired loading pressure and click Execute. For the test at 1000 psi, select 1000 psi. A window pops up, click run to start the test and the system begins lowering the press and applying pressure. Make sure the back-pressure regulator is open so any trapped air may escape the system.

19) Monitor the system as pressure increases, being sure the press doesn't exceed the designated closure stress.
20) Once the desired closure stress is reached, close the back-pressure regulator valve.
21) Zero the pressure sensors by going to Tools, selecting Inputs Offsets, and clicking the zero next to Differential Pressure and Cell Pressure.
22) Open the nitrogen cylinder by screwing the cap to the left (**Figure 17)**.

Figure 17: Experimental setup showing the gas cylinders and flow gauges.

23) Very slowly, screw the nitrogen tank regulator to the right to allow nitrogen to flow into the cell. Pressurize the cell to a cell pressure of 30 psi using the digital view on the GCTS Testing Systems Computer Aided Testing Systems Software. To prevent blowing the proppant out of the cell, do not exceed a flowrate of 0.1 L/min.

24) Once a pressure of 30 psi has been reached, stop twisting the nitrogen tank pressure regulator and allow the flowrate to stabilize. While waiting, squirt soapy water onto all the fittings to check for any gas leak off. If gas isn't detected escaping, record the stabilized flowrate

as leak off. This is typically 0.1 L/min. If gas is detected escaping (air bubbles form in the soapy water), tighten the fitting until gas is no longer detected escaping.

25) Record the piston displacement.

26) To allow flow through the cell, slowly open the back-pressure regulator valve until a desired flowrate or differential pressure is reached. Note that the flowrate should not exceed 2 L/min and that the differential pressure should not exceed 2 psi or the transducer membrane may be damaged or become uncalibrated. A differential pressure of 0.100 psi was desired for the first reading. The same starting flowrate should be used for each stage.

27) Record the flowrate, cell pressure, and differential pressure at the target differential pressure or flowrate.

28) Take four measurements at four different flowrates at each closure stress. To establish target pressure drops for average fracture conductivity measurements, divide the first differential pressure by four.

29) Slowly close the back-pressure regulator until the next differential pressure reaches the target differential pressure.

30) Record the flowrate, cell pressure, and differential pressure readings. Repeat this process until four conductivity calculations are performed at the desired closure stress.

31) Once four readings have been measured, close the nitrogen tank regulator valve to close the system off from the nitrogen tank and allow the test cell to depressurize to 0 psi.
32) In the GCTS Testing Systems Computer Aided Testing Systems software, click Stop to end the test.
33) On the Projects screen, click the right arrow and select the next desired closure stress. Execute the test and the system begins to load to the next closure stress. Repeat 23 to 33 until measurements for the last desired closure stress have been taken.
34) Once the final measurements have been recorded, close the nitrogen cylinder, and let the system depressurize.
35) Reduce the closure stress to 500 psi and begin disassembling the test cell.
36) Once the axial displacement is about 0 mm, shut the pump off.
37) To turn the controller off, select File and then select Shut Down Controller. Turn off the controller once the Interlock light is lit.
38) Using compressed air, remove the top piston by blowing the air into the relief valve. To remove the bottom piston and the sample, use a hydraulic press and gently push the bottom piston and the sample out.

2.3.4.2. Procedure for Using the Same Sample

The reuse of a rock sample is beneficial as it allows for more tests to be performed while saving money on rock sample preparation as two tests are performed on

the same rock sample. The fracture conductivity testing procedure described in **Section 2.3.4.1.** is used to test conductivity, but the closure stresses used differ for the first conductivity test. To perform two tests on the same rock sample, a propped conductivity test is performed starting at 750 psi closure stress and going up to 2000 psi closure stress in 250 psi increments. Four points are required to predict the conductivity at higher closure stresses and the test may be stopped at 1500 psi if the slope of the four points shows an exponential decline on a semi-log plot where closure stress is plotted on the x-axis and conductivity is plotted on the y-axis. It is important to not go over 2000 psi closure stress as the rock won't be able to withstand retesting. Once the propped conductivity has been found at the low closure stresses, the sample is acidized and retested up to 6000 psi closure stress or fracture collapse to evaluate the conductivity of an acid fracture or an acid plus proppant fracture.

2.4. Design Considerations and Experimental Challenges

The chance of user error is high due to the number of steps required to prepare the sample and execute the fracture conductivity experiment. While designing and working through the experimental procedures, the following were considered:

1) To maintain cell pressure and prevent leak off or gas channeling around the test sample, an even coating of epoxy needs to be around the sample. All fittings should be securely fastened.
2) If the sample is jostled during preparation or experiment set-up, the uniform proppant distribution may no longer be maintained which impacts the test results as proppant channeling may occur. Consistent

preparation of the sample and test as well as proppant distribution is needed to properly compare results from different tests.

3) The fracture must be completely sealed off during the epoxy process. If any epoxy leaks into the fracture, conductivity results may become skewed. To ensure no epoxy leaks into the fracture, the tape must be glued and smoothed out.
4) During test cell pressurization, the nitrogen flowrate should be closely monitored and not allowed to exceed 0.1 L/min to prevent proppant from being blown out.

2.5. Experimental Conditions

Table 1 below summarizes the experimental conditions for this study. The same limestone outcrop was used for each test and nitrogen gas was the fluid used to test conductivity. SM Energy supplied 40/70 mesh proppant used for this study at a concentration of 0.2 lb/ft^2.

Table 1: Fracture conductivity experimental conditions.

Experiment Number	Rock Type	Fluid Type	Proppant Type and Concentration	Acid Type and Concentration	Acid Residence Time
1	Limestone, 99.4% Calcite	Nitrogen Gas	40/70 mesh, 0.2 lb/ft^2	N/A	N/A
2	Limestone, 99.4% Calcite	Nitrogen Gas	40/70 mesh, 0.2 lb/ft^2	N/A	N/A
3	Limestone, 99.4% Calcite	Nitrogen Gas	N/A	15% HCl	10 minutes
4	Limestone, 99.4% Calcite	Nitrogen Gas	40/70 mesh, 0.2 lb/ft^2	15% HCl	10 minutes
5	Limestone, 99.4% Calcite	Nitrogen Gas	40/70 mesh, 0.2 lb/ft^2	15% HCl	20 minutes
6	Limestone, 99.4% Calcite	Nitrogen Gas	40/70 mesh, 0.2 lb/ft^2	15% HCl	20 minutes
7	Limestone, 99.4% Calcite	Nitrogen Gas	40/70 mesh, 0.2 lb/ft^2	15% HCl	1.5 minutes
8	Limestone, 99.4% Calcite	Nitrogen Gas	40/70 mesh, 0.2 lb/ft^2	15% HCl	1.5 minutes

3. RESULTS

3.1. Introduction

This section discusses the results of the experiments and compares the surface profilometer scans taken before and after the samples were tested.

3.2. Proppant Size Analysis

A sieve analysis was conducted after each test with proppant to compare the grain size distribution from before and after testing to analyze proppant crushing under closure stress.

3.2.1. Grain Size Analysis of the Proppant Only Tests

Figures 18 and 19 show the sieve analysis results for the two proppant only conductivity tests, with one fracture surface being smooth and the other fracture surface being rough. Both tests show a decrease in the 40-mesh and 50-mesh grain sizes and an increase in the pan grain sizes, which are grains smaller than a 140-mesh grain size. The test with the smooth fracture surface shows more crushing of the 80-and 100-mesh grains and an increase in the 120-mesh and 140-mesh grains while the test with the rough fracture surface shows less crushing in those grain sizes. Both samples were tested up to 6000 psi closure stress.

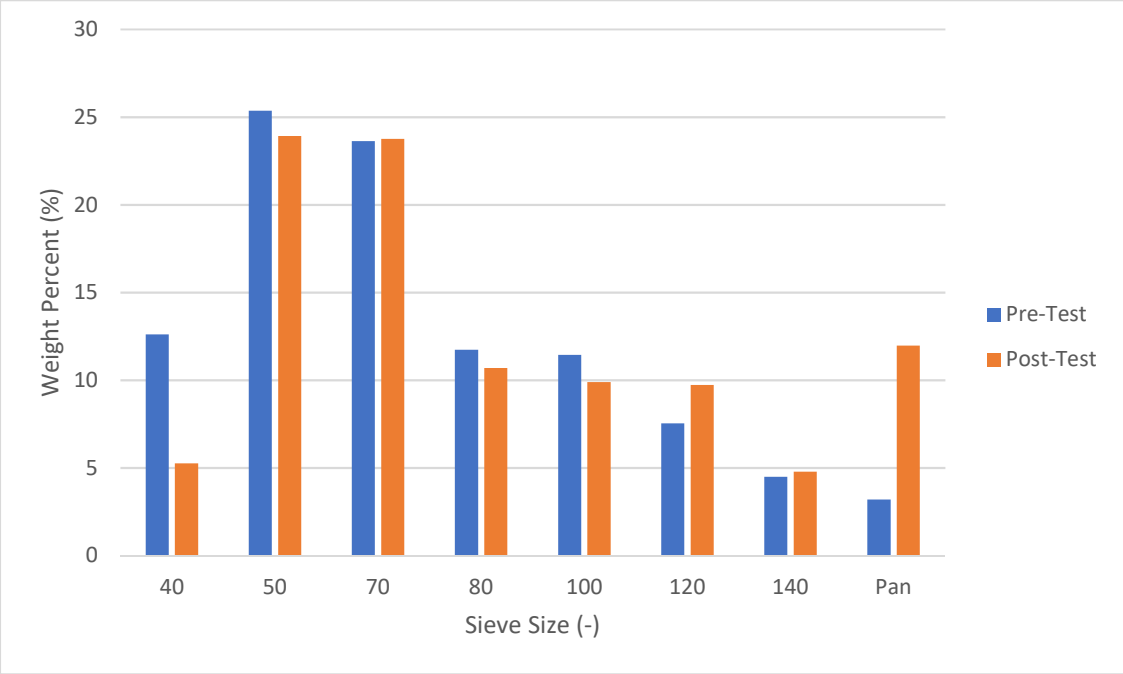

Figure 18: Sieve analysis of smooth cut sample proppant only.

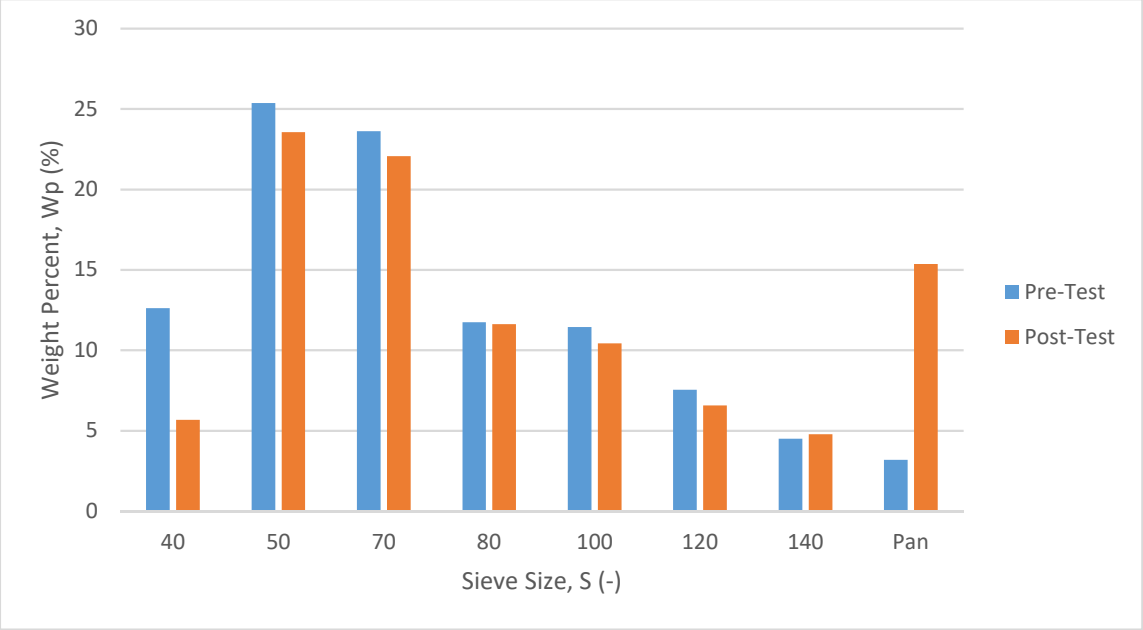

Figure 19: Sieve analysis of fractured sample proppant only.

3.2.2. Grain Size Analysis of Acid + Proppant Tests

Figure 20 presents the grain size distribution for the 10-minute residence time acid flush with 0.2 lb_m/ft^2 of 40/70 mesh proppant. This test went up to a closure stress of 8000 psi and shows similar behavior to the proppant only tests as described above where there was a decrease in the 40-mesh grain sizes and a significant increase in the pan grain sizes. The 70-mesh to 140-mesh grains also saw a decrease while the 50-mesh grain size increased.

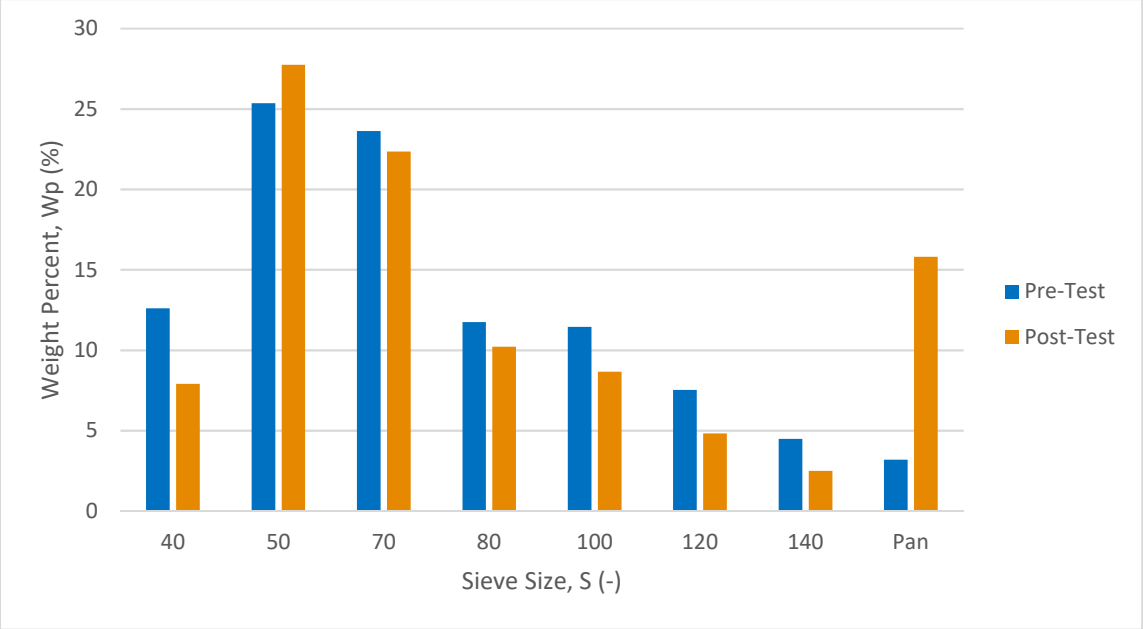

Figure 20: Sieve analysis of 10-minute residence time propped sample.

Figures 21 and 22 show the sieve analyses of the two 20-minute residence time acid flush plus 0.2 lb_m/ft^2 of 40/70 mesh proppant. **Figure 21** shows the first test, which was conducted up to a closure stress of 4000 psi while **Figure 22** shows the second test which was conducted up to a closure stress of 3000 psi. The fracture was no longer supported at these closure stresses so testing was stopped. As with the tests, grain sizes

from 70-mesh to 140-mesh saw a decrease while there was an increase in the pan sized grains, although the second test showed the least increase in pan sized grains as compared with all other tests. There was a notable increase in the 40-mesh grain sizes in both tests and the 50-mesh grain size in the second test. This was due to fragments of the rock sample being collected, sieved, and weighed with the proppant.

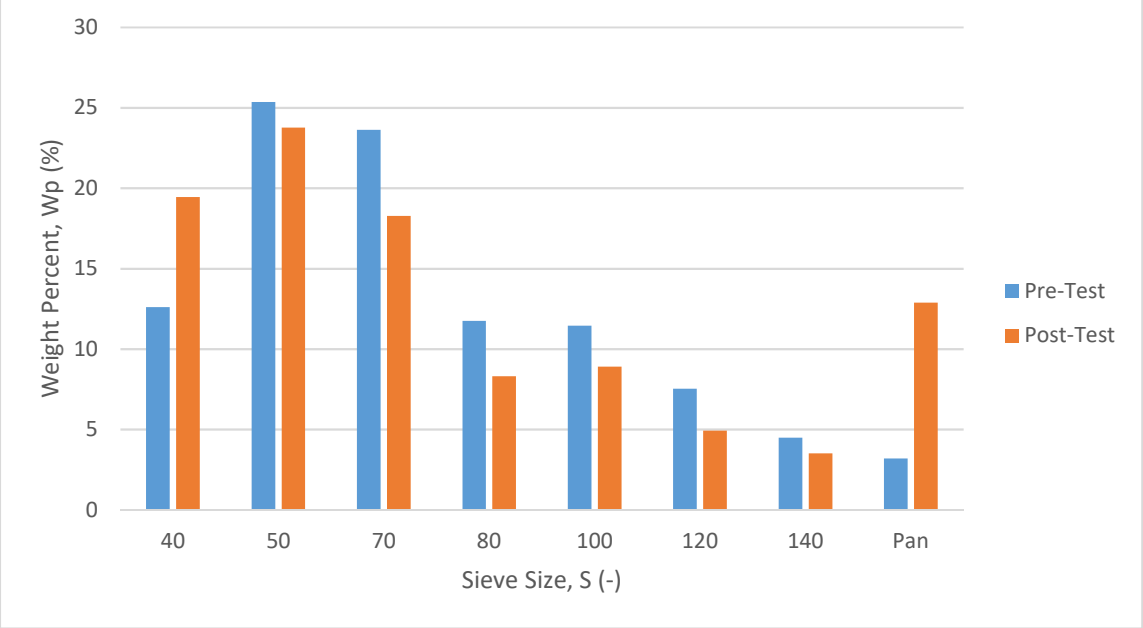

Figure 21: Sieve analysis of 20-minute residence time propped sample Test 1.

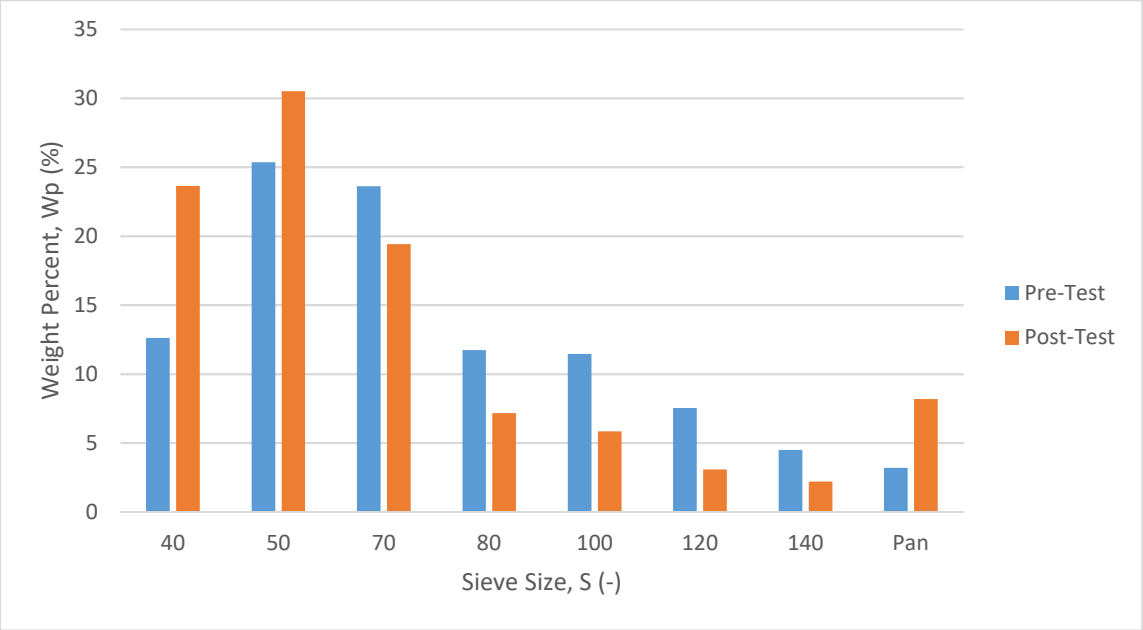

Figure 22: Sieve analysis of 20-minute residence time propped sample Test 2.

Figures 23 and 24 show the grain size distributions for the two 1.5-minute residence time plus 0.2 lb_m/ft^2 of 40/70 mesh proppant. Each sample was taken up to a closure stress of 6000 psi. They agree with the previous grain distributions by showing a decrease in most grain sizes while increasing the pan grain sizes. The second test showed an increase in 50-mesh grains as with the 10-minute residence time sample. Overall, the proppant showed a tendency to crush, producing more fine sized particles even at closure stresses as low as 3000 psi. The most fines produced came at the highest closure stress of 8000 psi as seen in **Figure 20**.

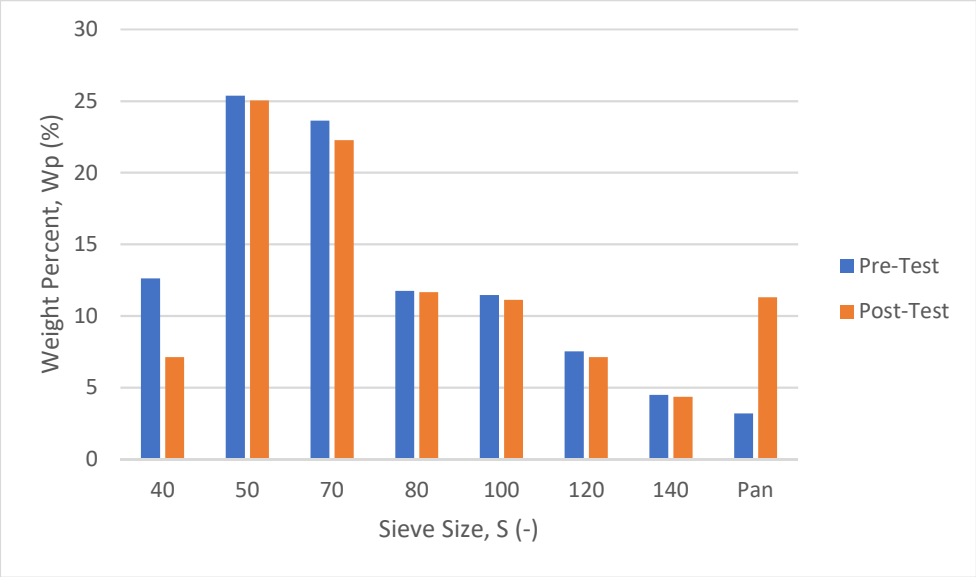

Figure 23: Sieve analysis of 1.5-minute residence time propped sample Test 1.

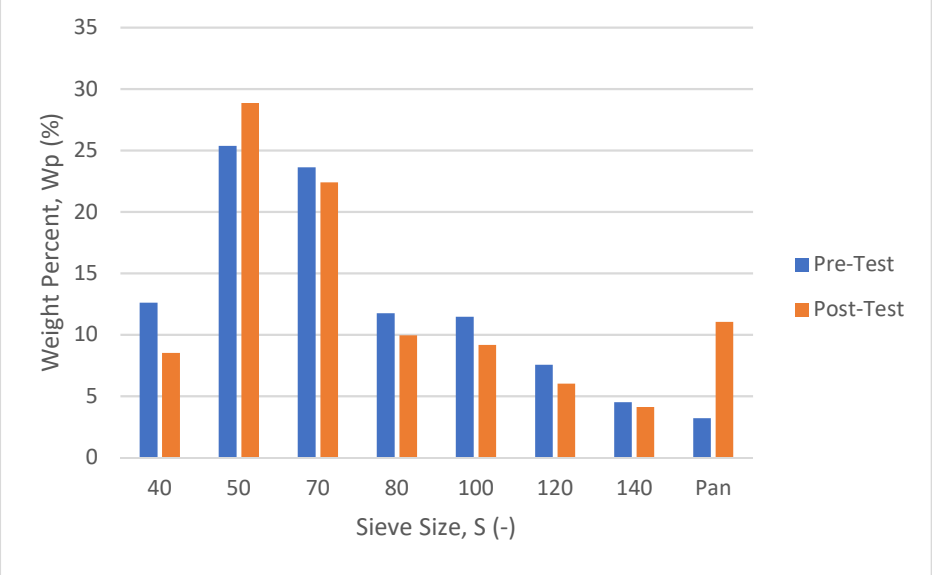

Figure 24: Sieve analysis of 1.5-minute residence time propped sample Test 2.

3.3. Surface Analysis

Figure 25 shows the damaged samples. 20-minute residence time acid fracture samples (**Figure 25 c and d**) show significantly more crushing and damage to the sample as compared with the smooth cut sample with proppant only and the 10-minute residence time sample (**Figure 25 a and b**). **Figure 25 c and d** also show how the proppant was impacted during the test by the flow of nitrogen gas and the closure stress applied to the sample with channels forming throughout the proppant pack and proppant settling in acid etched slumps in the fracture surface.

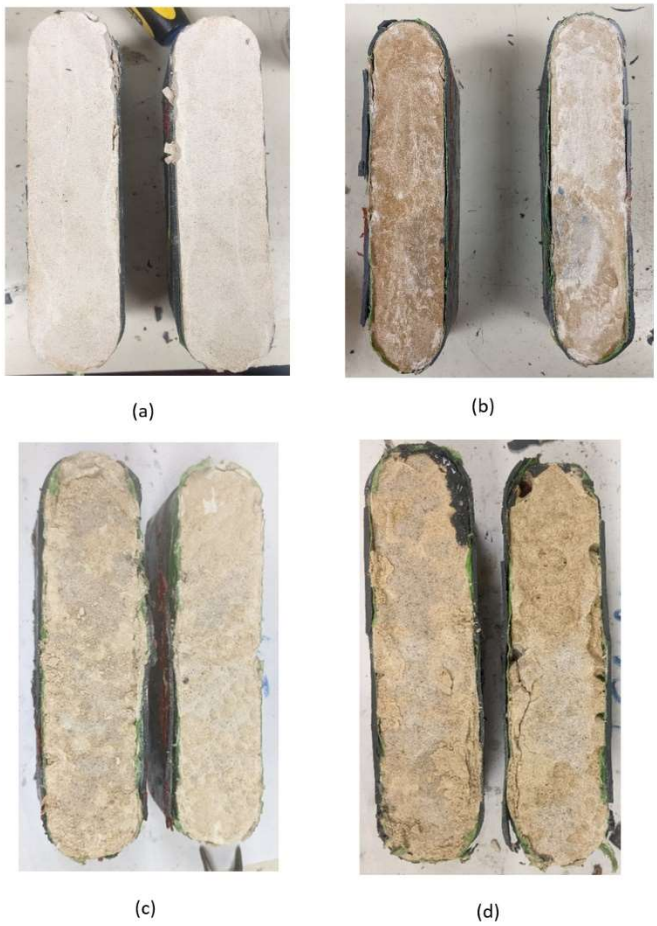

Figure 25: Pictures of test samples after conductivity testing with a) the smooth cut proppant only test b) the 10-minute residence time propped sample c) the first 20-minute residence time propped sample and d) the second 20-minute residence time propped test.

As explained in Section 2.2.2, a laser profilometer was used to scan the surface of the fracture to generate a 3-dimensional profile using the output measurements and MATLAB code. Scans were taken of the sample surfaces before and after conductivity testing.

3.3.1. Surface Scans of Proppant Only Tests

Figure 26 shows the 3-dimensional profile of the smooth surface proppant only conductivity test after the experiment was performed. The before scans were not taken as the sample surface was flat. While there are some minor changes to the edges and the flat surface, the sample for the most part remained intact and unchanged. **Figure 27** shows the 3-dimensional profile of the rough surface proppant only conductivity test. Minor changes can be seen on the high points of each half of the sample with the middle of top showing a decrease in high points and the left side of the bottom showing a decrease in high points. It is expected that high points will crush as closure stress is applied and increased.

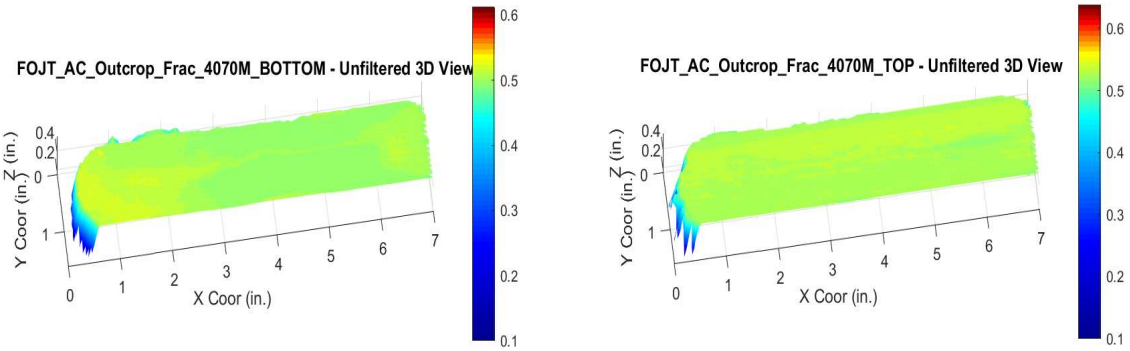

Figure 26: Post-test scans of smooth cut surface after conductivity testing.

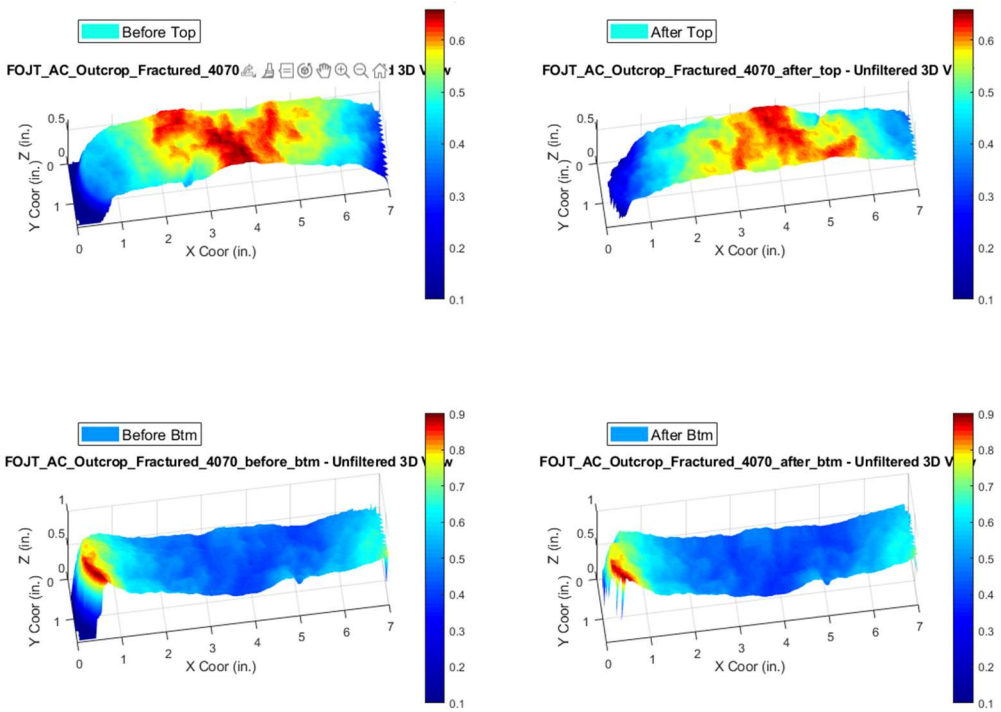

Figure 27: Post-test scans of the fractured surface after conductivity testing.

3.3.2. Surface Scans of Acid and Acid + Proppant Tests

Figures 28 shows the 10-minute residence time test and **Figure 29** shows the 10-minute residence time plus 0.2 lb_m/ft^2 of 40/70 mesh proppant 3-dimensional surface profiles. The left side of each figure shows the sample after the acid flush and the right side shows the sample after proppant was added and conductivity testing performed. In both **Figures 28 and 29** minor dissolution can be seen with localized high points occurring along the sample and around the edge of the sample. While the fracture surface in **Figure 28** didn't change much, the fracture surface in **Figure 29** changed noticeably with more high points being found on the top of the sample, indicative of

proppant embedment, while the bottom of the sample experienced crushing along the top edge.

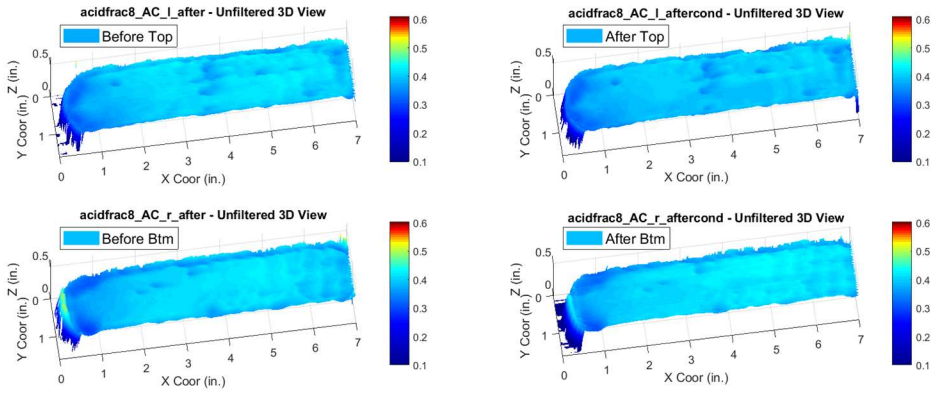

Figure 28: Post-test scans of the 10-minute residence time acid fracture.

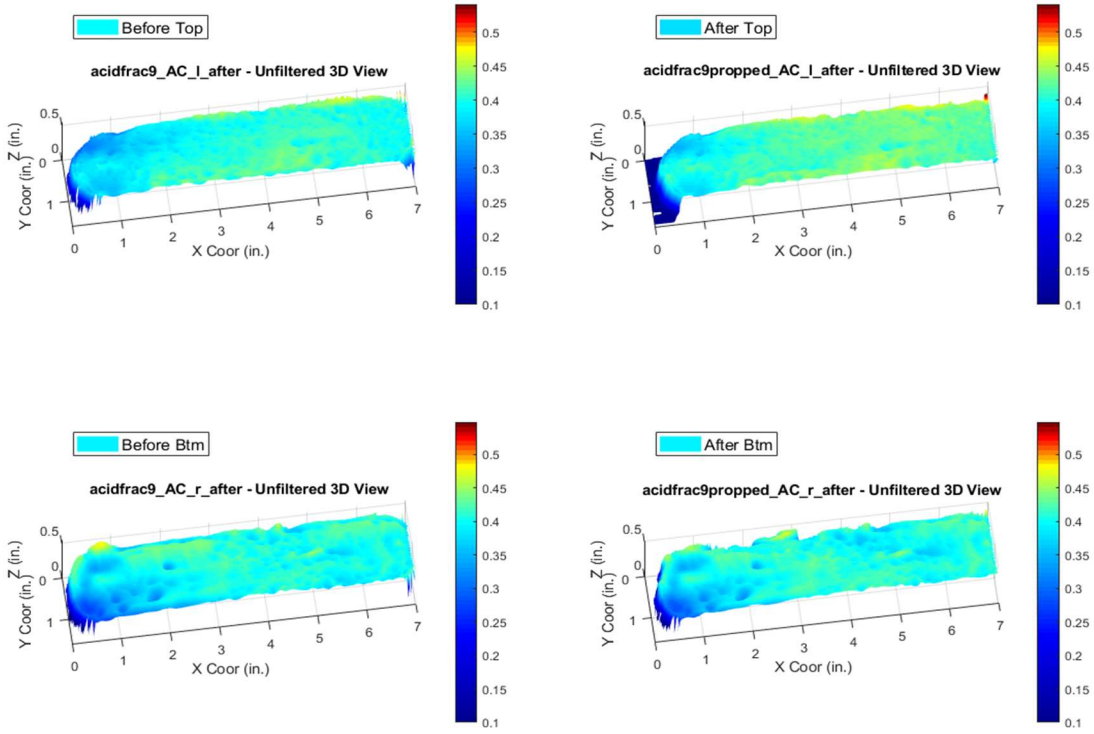

Figure 29: Post-test scans of the 10-minute residence time propped acid fracture.

Figures 30 and Figure 31 show the 20-minute residence time plus 0.2 lb_m/ft^2 of 40/70 mesh proppant 3-dimensional surface profiles. The left side of each figure shows the sample after the acid flush and the right side shows the sample after proppant was added and conductivity testing performed. Compared with the 10-minute residence time, significant dissolution was seen after the acid flush. Severe crushing of high points is also seen in both samples with the bottom of each sample being significantly flatter after conductivity testing. The top of each sample also experienced flattening, with the second test showing more flattening of the fracture surface than the first test. As the high points collapse, the fracture loses support and a decrease in conductivity is expected. This is seen in the conductivity results presented in Section 3.4.

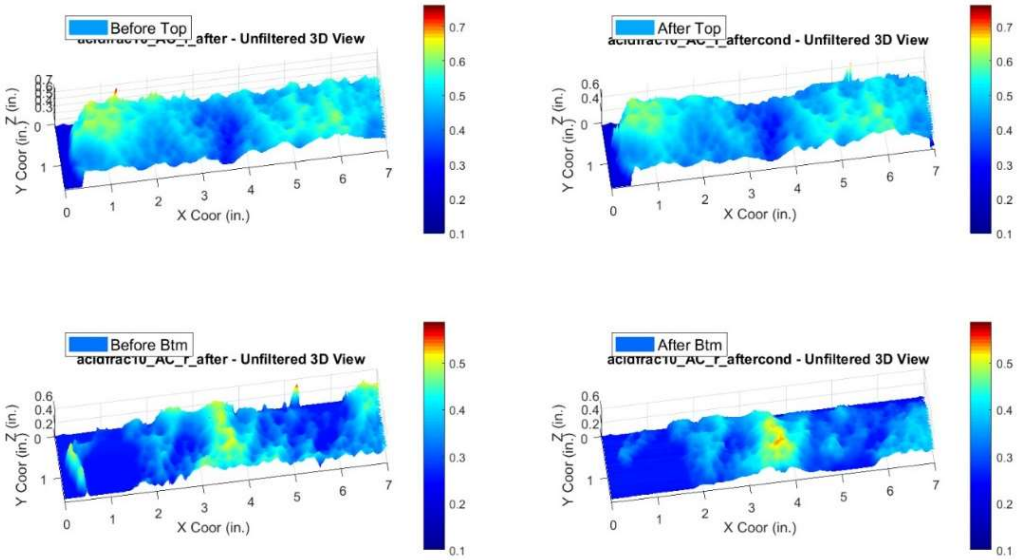

Figure 30: Post-test scans of the 20-minute residence time propped acid fracture Test 1.

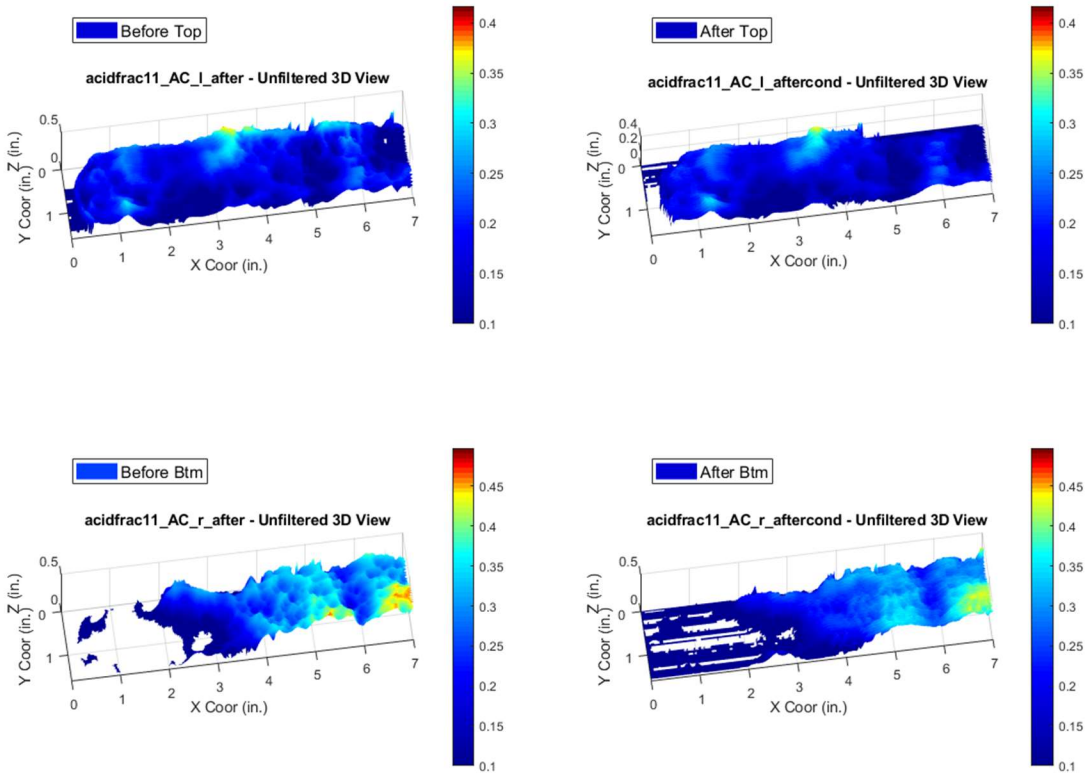

Figure 31: Post-test scans of the 20-minute residence time propped acid fracture Test 2.

Figures 32 and Figure 33 show the 1.5-minute residence time plus 0.2 lb_m/ft^2 of 40/70 mesh proppant 3-dimensional surface profiles. The left side of each figure shows the sample after the acid flush and the right side shows the sample after proppant was added and conductivity testing performed. Both tests show minor changes in the fracture surface and appear mostly unchanged throughout testing. Importantly however, **Figure 33** shows that small channels were created during the acid flush which led to an increase in conductivity as seen in Section 3.4.

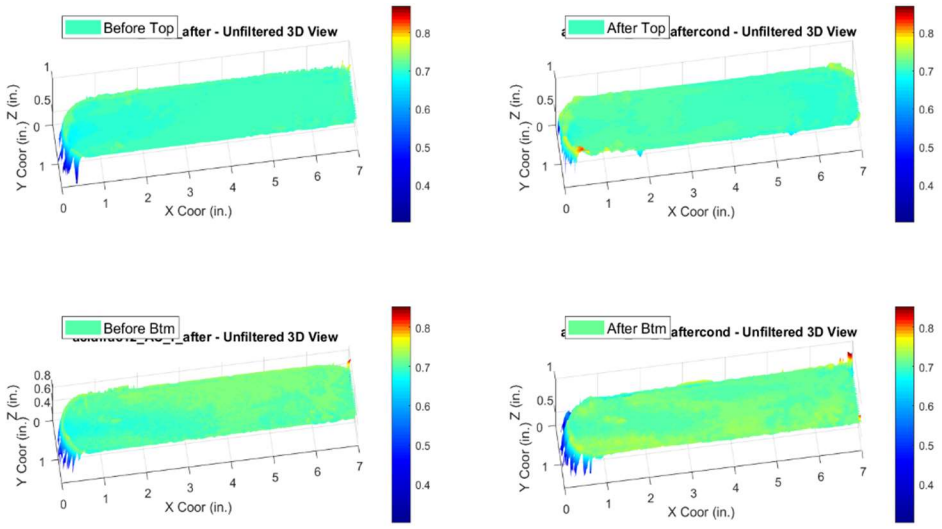

Figure 32: Post-test scans of the 1.5-minute residence time propped acid fracture Test 1.

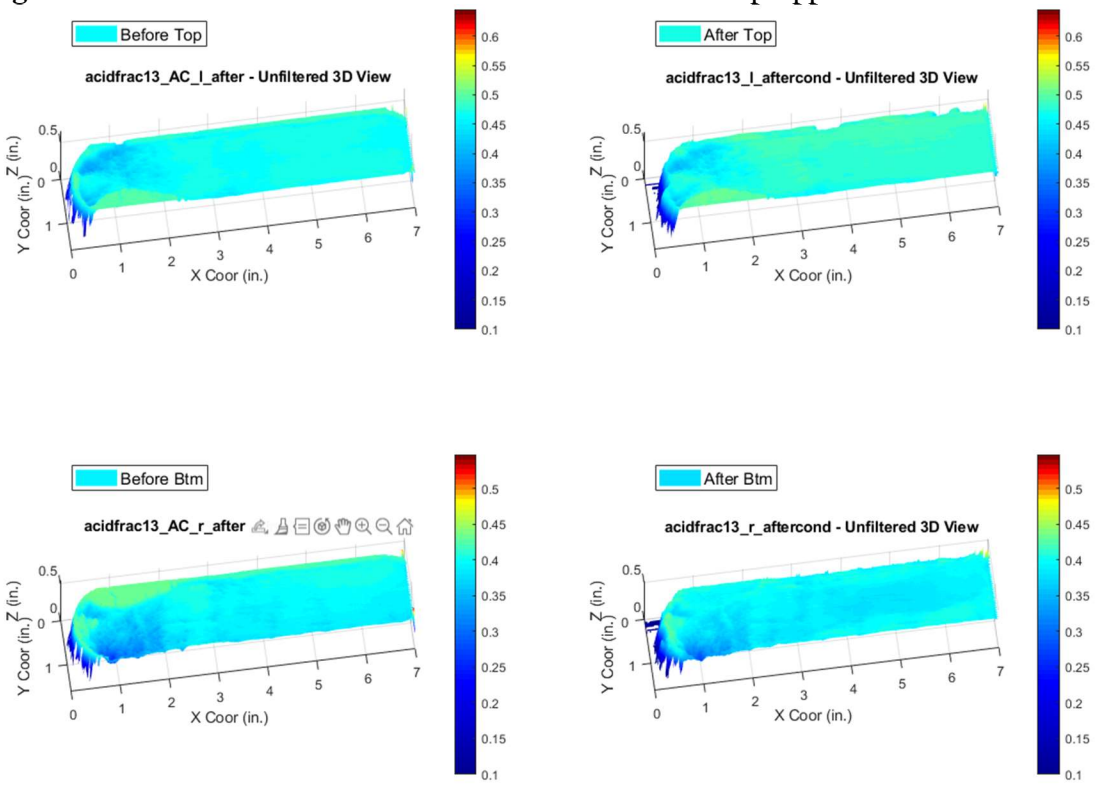

Figure 33: Post-test scans of the 1.5-minute residence time propped acid fracture Test 2.

3.3.3. Volumetric Change Calculations

A laser profilometer was used to scan the surface of the fracture to generate a 3-dimensional profile and calculate surface volume changes using the output measurements and MATLAB code for both the stop and the bottom of the sample. The results are presented in **Table 2**. This method of analysis only captured surface changes which would only account for proppant embedment above the fracture surface. Any proppant that was embedded into the sample and below the fracture surface is not considered. Furthermore, the calculation is skewed due to the behavior of the rock under stress with tendencies to fracture and fragment, especially around the edges of the sample as seen in **Figure 25**, leading to the results being unreliable.

Table 2: Volume change calculation results from MATLAB code.

				Volume Change (in^3)	
Sample Number	**Sample Type**	**Proppant**	**Acid**	**Bottom**	**Top**
1	Smooth	Provided 40/70 mesh	N/A	-0.1589	0.2503
2	Fractured	Provided 40/70 mesh	N/A	-0.0129	0.3240
3	Smooth	N/A	10-minutes, 15% HCl	0.0139	-0.0598
4	Smooth	Provided 40/70 mesh	10-minutes, 15% HCl	0.0770	-0.0239
5	Fractured	Provided 40/70 mesh	20-minutes, 15% HCl	0.0938	-0.0490
6	Fractured	Provided 40/70 mesh	20-minutes, 15% HCl	0.0395	0.2168
7	Smooth	Provided 40/70 mesh	1.5-minutes, 15% HCl	-0.4464	-0.6672
8	Smooth	Provided 40/70 mesh	1.5-minutes, 15% HCl	0.1961	-0.0347

3.4. Conductivity Analysis

The following section provides the calculated fracture conductivity values for the baseline propped limestone sample and the baseline limestone acid fracture sample. Most samples were loaded to a closure stress of 6000 psi. The proppant concentration was 0.2 lb_m/ft^2 and the acid injected to create the acid fracture was 15% hydrochloric acid with a residence time of 10 minutes. Baseline conductivity values were found to compare with samples that were acid fractured and propped to determine what benefit, if any, there is in combining both fracturing methods.

3.4.1. Acid Fracture Conductivity

One sample was made with limestone outcrop and a smooth fracture surface. The sample was acid fractured with 15% hydrochloric acid for a residence time of 10 minutes. **Figure 34** presents the conductivity values calculated using **Eq. 12** at each closure stress. The conductivity decreased exponentially on a semi-log scale as closure stress increased. Conductivity values could not be calculated for the 1000 psi and 2000 psi closure stresses as the differential pressure was too small to be accurately read by the Validyne DP 15 pressure transducer. An exponential line was fitted through the data to estimate the conductivity at the lower closure stresses. The conductivity decrease came from the etched fracture surface collapsing, indicating that acid fracture conductivity is dependent on the mineralogy of the rock. Streaks of non-dissolvable rock support the fracture and provide relatively high conductivity compared to the

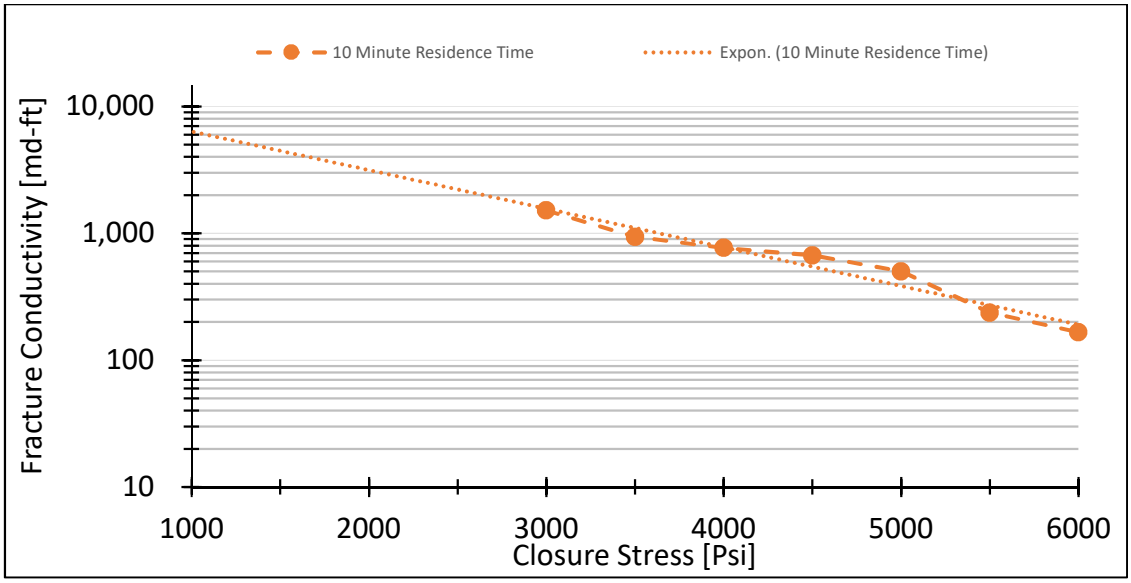

Figure 34: Calculated acid fracture conductivity values for limestone outcrop with 15% hydrochloric acid with a 10-minute residence time.

3.4.2. Propped Fracture Conductivity Results

Two samples were made with limestone outcrop with a smooth fracture surface. **Figure 35** presents the conductivity values calculated using **Eq. 12** at each closure stress. The conductivity decreased exponentially on a semi-log scale as closure stress increased. In Test 1, there was a dip in conductivity at 4000 psi followed by a recovery. This was caused by one of the pressure transducers being plugged, artificially creating a higher differential pressure than the sample experienced. Conductivity recovered and followed the exponential decline trend that was present from 1000 psi to 3500 psi. Conductivity decline occurred due to the proppant pack being crushed under closure stress, preventing the proppant's ability to support the fracture and allow flow. Conductivity values for the propped samples are lower than the conductivity found with the acid fracture sample tested above. The second conductivity test showed a drastic decrease in conductivity at 5000 as compared with the first conductivity test performed.

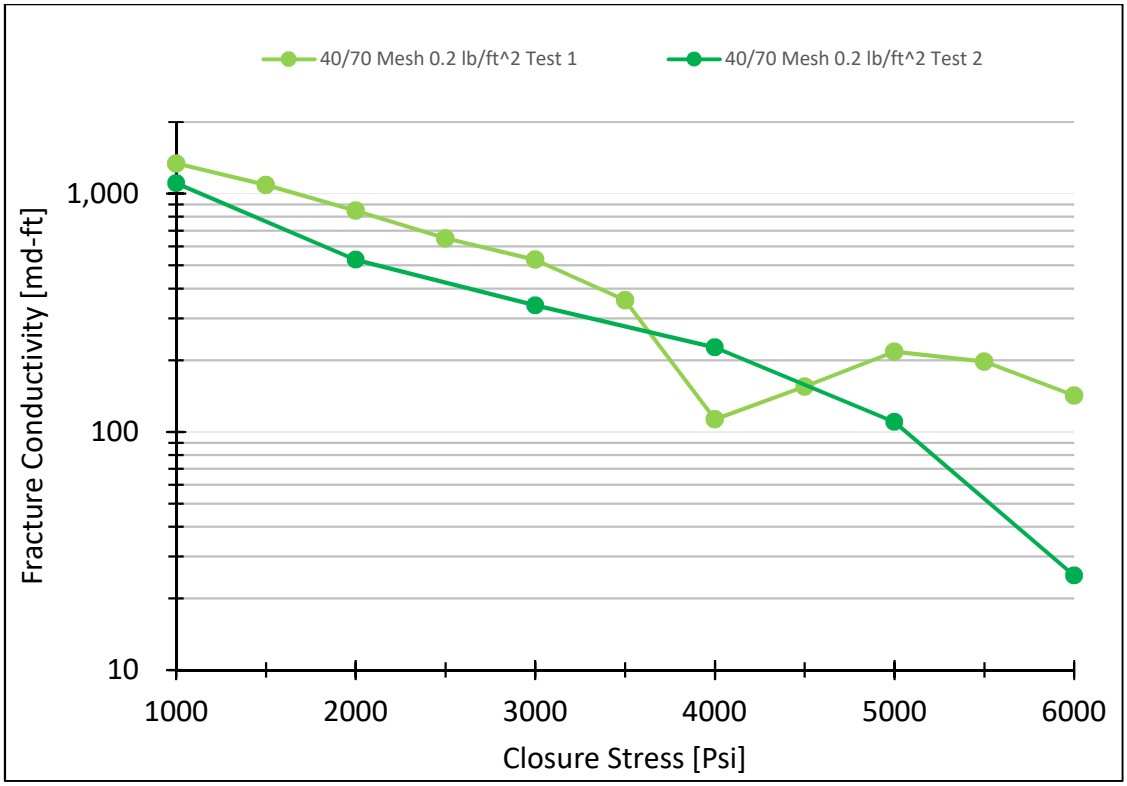

Figure 35: Calculated conductivity values for limestone outcrop with 0.2 lb/ft^2 40/70 mesh.

3.4.3. Propped Acid Fracture Conductivity Results

Three limestone outcrop samples were tested using a combined method of acid fracturing and proppant packing with 0.2 lb/ft^2 of 40/70 mesh sand. One sample was acid fractured using a residence time of 10 minutes and two samples were acid fractured using a residence time of 20 minutes. **Figure 36** shows the results of all the propped acid fracture tests. The sample that had a 10-minute acid residence time exhibited high conductivity values and an exponential decline on a semi-log scale. The 20-minute residence time samples had more varied results. Both samples had an initially high conductivity and then experienced a step change decrease resulting in drastically lower conductivities as compared with the 10-minute residence time sample. The 10-minute

residence time propped sample has conductivity values higher than samples that only had proppant in them and values similar to the sample that was acid fractured with a 10-minute residence time. The first 20-minute residence time sample had lower conductivities at all closure stresses as compared with the proppant only sample. The second 20-minute residence time sample had an initial conductivity higher than the proppant only samples, but had lower conductivities at higher closure stresses. Both 20-minute residence time samples had rapid conductivity decline and were not tested out to 6000 psi as the rest of the samples were. The 1.5-minute residence time samples showed variety with the first test showing a lower conductivity than the 10-minute residence time, but maintaining a steady decline at a similar slope to the 10-minute residence time. The second 1.5-minute residence time test showed an initially higher conductivity due to small channels being etched into the fracture. At higher closure stress however, the conductivity values dropped below the values of the 10-minute residence time.

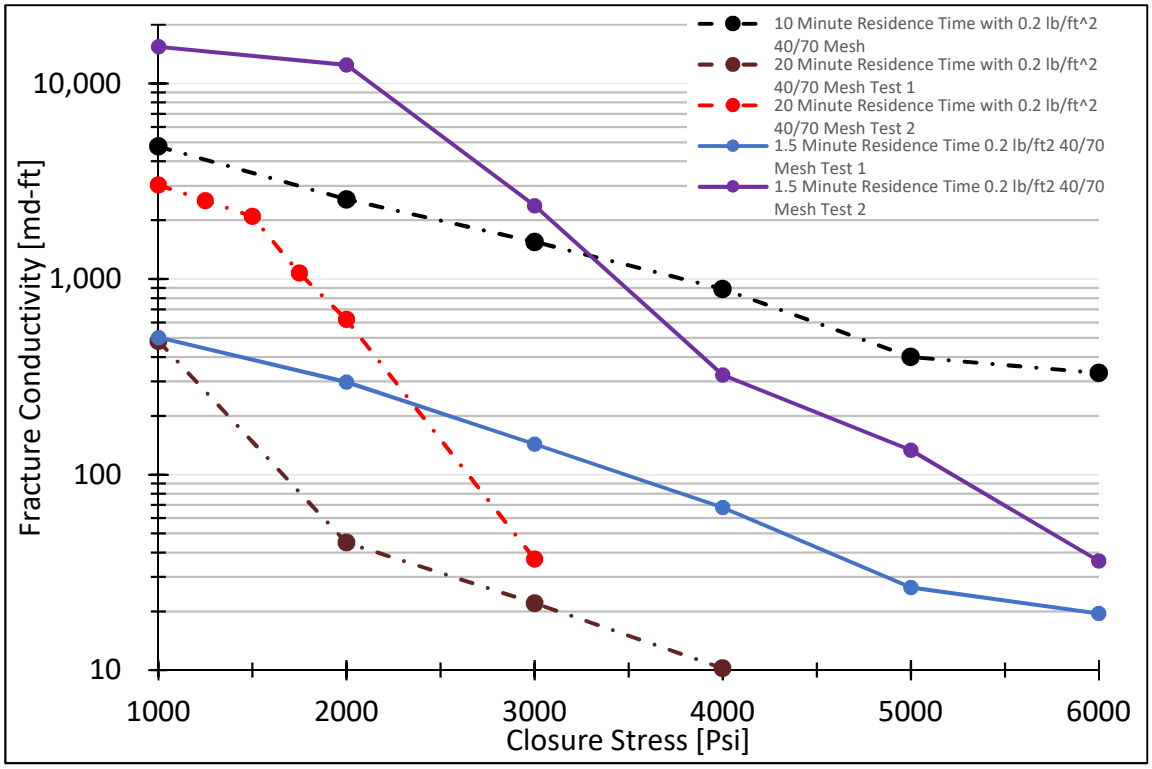

Figure 36: Calculated conductivity values for acid fractured samples with 0.2 lb/ft2 40/70 mesh proppant.

3.4.4. Combined Conductivity Results

Figure 37 presents the combined conductivity results of all limestone outcrop samples. The 10-minute residence time acid sample and the 10-minute residence time acid sample with 0.2 lb/ft^2 40/70 mesh proppant not only had similar conductivity values and declines, but they also exhibited the highest conductivity values. The sample that had the proppant in it importantly had higher conductivity at 6000 psi closure stress with a cross-over occurring just after 5000 psi of closure stress. Samples not acidized but propped with 0.2 lb/ft^2 40/70 mesh sand showed a steady decline and had conductivity values between the 10-minute residence time samples and the 20-minute residence time samples, which had the lowest conductivity values of all the tests conducted. The 20-

minute residence time samples were also more varied in conductivity values as compared with the other samples and had steeper declines. Notably, the 20-minute residence time samples were not tested out to 6000 psi due to the decline in conductivity. Furthermore, the first 1.5-minute residence time test shows the minimum conductivity of the proppant pack as the fracture surface was almost smooth and wouldn't have supported the fracture open as much as the proppant. The second 1.5-minute residence time test shows the benefits of having acidized channels as the initial conductivity values at lower closure stresses were significantly higher than all other tests. As closure stress increased however, the conductivity aligned more with the proppant only conductivities as the support mechanism of the fracture changed from acid etched to proppant supported.

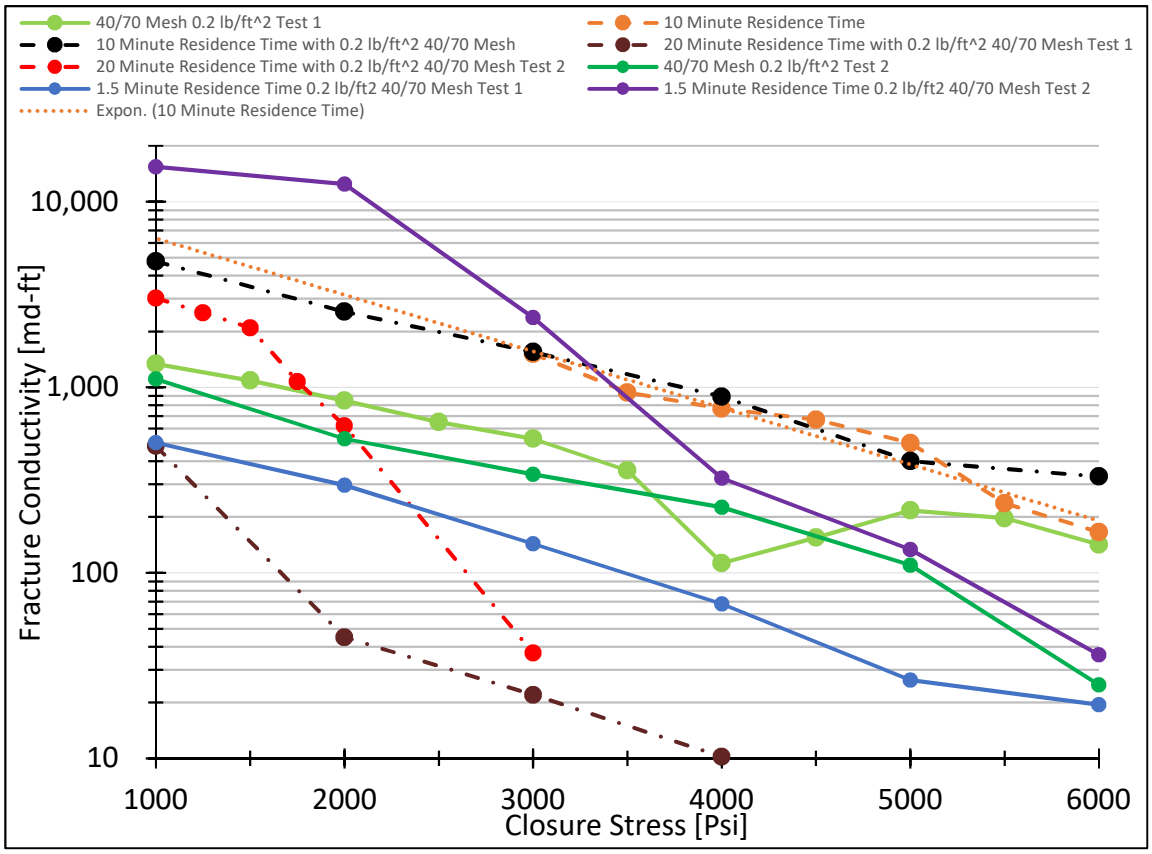

Figure 37: Combined calculated conductivity values from all tests performed.

4. CONCLUSIONS

4.1. Conclusions

A study was conducted to determine the fracture conductivity of limestone outcrop samples while analyzing the impact an acid pre-flush would have on conductivity. Values were measured for outcrop samples that were propped with 40/70 mesh sand and acid fractured with 15% hydrochloric acid. While the focus was on how the proppant would perform and what impact the acid would have, changes in the fracture surface were also analyzed.

This thesis presents the experimental design and methodology used to quantify fracture conductivity from the pre-experimental preparation to the post-experimental analysis of the results. Samples with lower acid residence times showed higher conductivity values and more stable declines.

The following conclusions were made from an in-depth analysis of the results:

1) Acid fracture conductivity is higher at all closure stresses than propped fracture conductivity for the limestone outcrop compared with a 40/70 mesh sand.
2) Higher acid residence times correspond with lower conductivity values as the fracture cannot be supported by the rock or proppant after being acid fractured. Higher residence times also correspond to steeper declines in conductivity and increased variability as compared with other samples.

3) Proppant supports the acid fracture for the 10-minute residence time sample and allows for higher conductivity at higher closure stresses as compared to just an acid fractured sample.

4.2. Recommendations

An important limitation of this study was the quantity of samples tested and the validity of the results presented in this thesis can only be strengthened by performing more experiments.

Additional recommendations to consider for future work are as follows:

1) Use outcrop samples that are more representative of the formation of interest.

REFERENCES

Almubarak, Majed, Almubarak, Tariq, Ng, Jun Hong, Hernandez, Julio, and Hisham Nasr-El-Din. "Recent Advances in Waterless Fracturing Fluids: A Review." Paper presented at the Abu Dhabi International Petroleum Exhibition & Conference, Abu Dhabi, UAE, November 2020. DOI: 10.2118/202981-MS

ASTM Standard-C136M-19. 2019. Standard Test Method for Sieve Analysis of Fine and Coarse Aggregates. West Conshohocken, Pennsylvania, U.S.A.: ASTM International.

Clark, J.B., "A Hydraulic Process for Increasing the Productivity of Wells." J Pet Technol 1 (1949): 1–8. DOI: https://doi.org/10.2118/949001-G

Cooke Jr., C.E. 1973. Conductivity of Fracture Proppants in Multiple Layers. Journal of Petroleum Technology 25 (9): 1,101-1,107. DOI: 10.2118/4117-PA.

Cooke Jr., C.E. 1977. Fracturing with a High-Strength Proppant. Journal of Petroleum Technology 29 (10): 1,222-1,226. DOI: 10.2118/6213-PA.

Copeland, A. (2020). The Impact of Proppant Grain-size Distribution on Fracture Conductivity in Shale Formations. Texas A&M University, Petroleum Engineering, College Station.

Duenckel, R. J., Barree, R. D., Drylie, S., O'Connell, L. G., Abney, K. L., Conway, M. W., Moore, N., and F. Chen. "Proppants- What 30 Years of Study has Taught Us." Paper presented at the SPE Annual Technical Conference and Exhibition, San Antonio, Texas, USA, October 2017. doi: 10.2118/187451-MS

Fernandez, J (2019). A Study of a Multitude of Proppants for Fracture Conductivity of Unconventional Resources. MS Thesis, Texas A&M University, College Station, Texas, U.S.A. (May 2019)

Guerra, J. (2019). Fracture Conductivity Behavior in Shale Formations. PhD Dissertation, Texas A&M University, College Station, Texas, USA (August 2019).

Jin, X. (2020). Effect of Mineralogic Heterogeneity on Acid Fracturing Efficiency. PhD Dissertation, Texas A&M University, College Station, Texas, U.S.A. (August 2020)

Kamenov, A.N. 2013. The Effect of Proppant Size and Concentration on Hydraulic Fracture Conductivity in Shale Reservoirs. MS Thesis, Texas A&M University, College Station, Texas, U.S.A. (May 2013).

Larsen, D.G. and Smith, L.J. 1985. New Conductivity Found in Angular Blends of Fracturing Sand. Paper presented at the SPE Production Operations Symposium, Oklahoma City, Oklahoma, U.S.A., 10-12 March. Society of Petroleum Engineers. DOI: 10.2118/13814- MS.

Melendez, M. 2007. The Effects of Acid Contact Time and Rock Surfaces on Acid Fracture Conductivity. MS Thesis, Texas A&M University, College Station, Texas, U.S.A. (August 2007).

Neumann, L F, de Oliveira e Sousa, J L, Brandão, E M, and T J Oliveira. "Acid Fracturing: New Insights on Acid Etching Patterns from Experimental Investigation." Paper presented at the SPE Hydraulic Fracturing Technology

Conference, The Woodlands, Texas, USA, February 2012. doi: https://doi.org/10.2118/152179-MS

Palisch, T.T., Vincent, M., and Handren, P.J. 2010. Slickwater Fracturing: Food for Thought. SPE Production & Operations 25 (3): 327-344. DOI: 10.2118/115766-PA.

Wang, X. 2015. Acid Fracture and Fracture Conductivity Study on Heterogeneous Carbonate Rock Samples. MS Thesis, Texas A&M University, College Station, Texas, U.S.A. (December 2015).

Winner, R. 2018. A Study on the Effect of Water Damage to Fracture Conductivity in the Meramec Shale. MS Thesis, Texas A&M University, College Station, Texas, U.S.A. (August 2018).

Wylie, K. 2018. Experimental Evaluation of Novel Proppants for Use in Hydraulic Fracturing of Unconventional Reservoirs. MS Thesis, Texas A&M University, College Station, Texas, U.S.A. (May 2018).

Zhang, J. 2014. Creation and Impairment of Hydraulic Fracturing Conductivity in Shale Formations. PhD Dissertation, Texas A&M University, College Station, Texas, U.S.A. (August 2014).